Am J Physiol Gastrointest Liver Physiol 327: G438–G453, 2024.
First published June 11, 2024; doi:10.1152/ajpgi.00220.2023

american physiological society

AMERICAN JOURNAL OF PHYSIOLOGY
GASTROINTESTINAL AND LIVER PHYSIOLOGY

RESEARCH ARTICLE

Epithelial Cell Metabolism

Colonocyte keratins stabilize mitochondria and contribute to mitochondrial energy metabolism

Joel H. Nyström,[1] Taina R. H. Heikkilä,[1] Keshav Thapa,[1,2] Ilari Pulli,[1] Kid Törnquist,[1,3] and Diana M. Toivola[1,4,5]

[1]*Cell Biology, Biosciences, Faculty of Science and Engineering, Åbo Akademi University, Turku, Finland;* [2]*Research Centre for Integrative Physiology and Pharmacology, Institute of Biomedicine, University of Turku, Turku, Finland;* [3]*Minerva Foundation Institute for Medical Research, Biomedicum Helsinki, Helsinki, Finland;* [4]*InFLAMES Research Flagship Center, University of Turku and Åbo Akademi University, Turku, Finland; and* [5]*Turku Center for Disease Modeling, University of Turku, Turku, Finland*

Abstract

Keratin intermediate filaments form dynamic filamentous networks, which provide mechanical stability, scaffolding, and protection against stress to epithelial cells. Keratins and other intermediate filaments have been increasingly linked to the regulation of mitochondrial function and homeostasis in different tissues and cell types. While deletion of keratin 8 ($K8^{-/-}$) in mouse colon elicits a colitis-like phenotype, epithelial hyperproliferation, and blunted mitochondrial ketogenesis, the role of K8 in colonocyte mitochondrial function and energy metabolism is unknown. We used two K8 knockout mouse models and CRISPR/Cas9 $K8^{-/-}$ colorectal adenocarcinoma Caco-2 cells to answer this question. The results show that $K8^{-/-}$ colonocyte mitochondria in vivo are smaller and rounder and that mitochondrial motility is increased in $K8^{-/-}$ Caco-2 cells. Furthermore, $K8^{-/-}$ Caco-2 cells displayed diminished mitochondrial respiration and decreased mitochondrial membrane potential compared with controls, whereas glycolysis was not affected. The levels of mitochondrial respiratory chain complex proteins and mitochondrial regulatory proteins mitofusin-2 and prohibitin were decreased both in vitro in $K8^{-/-}$ Caco-2 cells and in vivo in $K8^{-/-}$ mouse colonocytes, and reexpression of K8 into $K8^{-/-}$ Caco-2 cells normalizes the mitofusin-2 levels. Mitochondrial Ca^{2+} is an important regulator of mitochondrial energy metabolism and homeostasis, and Caco-2 cells lacking K8 displayed decreased levels and altered dynamics of mitochondrial matrix and cytoplasmic Ca^{2+}. In summary, these novel findings attribute an important role for colonocyte K8 in stabilizing mitochondrial shape and movement and maintaining mitochondrial respiration and Ca^{2+} signaling. Further, how these metabolically compromised colonocytes are capable of hyperproliferating presents an intriguing question for future studies.

NEW & NOTEWORTHY In this study, we show that colonocyte intermediate filament protein keratin 8 is important for stabilizing mitochondria and maintaining mitochondrial energy metabolism, as keratin 8-deficient colonocytes display smaller, rounder, and more motile mitochondria, diminished mitochondrial respiration, and altered Ca^{2+} dynamics. Changes in fusion-regulating proteins are rescued with reexpression of keratin 8. These alterations in colonocyte mitochondrial homeostasis contribute to keratin 8-associated colitis pathophysiology.

colon; energy metabolism; inflammatory bowel diseases; keratins; mitochondria

INTRODUCTION

Keratins are intermediate filament (IF) proteins that assemble into dynamic filamentous networks in epithelial cells. Keratin filaments are formed through heteropolymerization of acidic type I keratins (K9-28) and basic/neutral type II keratins (K1-8 and K71-80) (1, 2). Keratin filaments in colon epithelial cells are composed of simple epithelial keratins, including type II keratin K8, and type I keratins K18, K19, and K20 (3). Keratins fulfill many functions in epithelial cells, including conveying protection against stress, providing mechanical integrity and protein and organelle scaffolding and targeting, and maintaining epithelial polarity and barrier function (3–5). In addition, keratins play an important role in maintaining mitochondrial and nuclear shape and function (6–9). The importance of keratins is evidenced by the many human skin and liver diseases associated with keratin mutations. While the role of keratin mutations in inflammatory bowel disease (IBD) remains ambiguous (5, 10–13), IBD patients were recently shown to neo-express K7

Correspondence: J. H. Nyström (joel.nystrom@abo.fi); D. M. Toivola (diana.toivola@abo.fi).
Submitted 5 October 2023 / Revised 30 May 2024 / Accepted 30 May 2024

in the colonic epithelium (14). However, a clear role for keratins in colonic health is observed in keratin 8 knockout ($K8^{-/-}$) mice, which display inflammation resembling human ulcerative colitis, epithelial hyperproliferation, disrupted barrier function, deregulated inflammatory signaling and differentiation, and unbalanced ion transport (15–20). Heterozygous K8 ($K8^{+/-}$) mice, which express ~50% less keratins than $K8^{+/+}$ mice, display an intermediate ion transport and hyperproliferation phenotype with no spontaneous inflammation but are more susceptible to chemically induced colitis (17, 21). In addition, $K8^{-/-}$ mouse colonocytes exhibit an energy metabolism phenotype characterized partly by reduced cellular uptake of the primary colonocyte energy source butyrate, a gut bacteria-produced short-chain fatty acid, and partly by diminished mitochondrial ketogenesis, a blunted ketogenic response, and fewer mitochondrial cristae (22).

Mitochondria are integral for normal cell function due to their central roles in cell metabolism (ATP synthesis), Ca^{2+} signaling and cell signaling cascades, cell fate, and redox homeostasis (23–25). The regulation of these cellular processes and the adaption of mitochondria to the metabolic needs of cells are achieved through dynamic regulation of mitochondrial distribution, fission and fusion, shape, and membrane composition (25). The regulation of mitochondria dynamics is complex, involving a multitude of both mitochondrial and nonmitochondrial proteins (24, 25). In recent years, IFs and IF-associated proteins, including neurofilaments, vimentin, desmin, and plectin, have increasingly been implicated in the regulation of mitochondrial dynamics and function (26, 27). In particular, a number of studies have highlighted an important role for keratins in maintaining mitochondrial shape, size, ultrastructure, motility, distribution, mitochondrial respiration, and/or mitochondrial membrane potential ($\Delta\Psi m$) in various epithelial cells from different tissues, including β-cells, hepatocytes, and keratinocytes (7, 8, 28–32).

Since colonocyte mitochondrial energy metabolism differs significantly from other organs due to the unique utilization of gut microbially produced metabolites for energy (33, 34), examining the role of keratins for colonocyte mitochondrial function is important. Our findings show that colonocyte keratins play a role in mitochondrial activity and dynamics, as the lack of K8 correlates with smaller, rounder, and more motile mitochondria in conjunction with diminished mitochondrial respiration. Intriguingly, we also found that mitochondrial and cytoplasmic Ca^{2+} dynamics are altered and Ca^{2+} levels are decreased upon K8 loss. These changes in mitochondrial dynamics and function may contribute to K8-associated colitis pathophysiology.

MATERIALS AND METHODS

Experimental Animals

$K8^{+/+}$, $K8^{+/-}$, and $K8^{-/-}$ mice in the FVB/n background (16) and $K8^{flox/flox}$ and $K8^{flox/flox}$;Villin-Cre mice in the C57BL/6 background ($K8^{flox/flox}$ mice were generated by and a kind gift from Karen Ridge (Northwestern University, Chicago, IL) (15) were used in the study. Genotyping was done using PuReTaq Ready-To-Go PCR Beads solution (Cytiva, Marlborough, MA). $K8^{+/+}$, $K8^{+/-}$ and $K8^{-/-}$ mice were genotyped utilizing the primers 0-neo-3: 5′-CCT GTC ATC TCA CCT TGC TCC TGC C-3′; Oea18: 5′-TTG GGT TAG GCC CTG CCT CTA GTG TCT-3′; and K8pcr: 5′-CGG TTA GTC GGG AAG AGA GGG GTC-3′ (16). Primers 5′-GCG TGG CTT TGG GAT TTA GAT TAG-3′ and 5′-CCT CCA GCC ATG TTT CTT TAT CTC-3′ for the flox transgene and 5′-GCG ATC GCT ATT TTC CAT GA-3′ and 5′-TCG ATG CAA CGA GTG ATG AG-3′ for the Cre transgene were used for genotyping $K8^{flox/flox}$ and $K8^{flox/flox}$;Villin-Cre mice (15). All mice were housed at the Central Animal Laboratory at the University of Turku and handled according to animal study protocols 197/04.10.07/2013, 3956/04.10.07/2016, ESAVI/16359/2019, and ESAVI/4498/2023 approved by the State Provincial Office of South Finland. Mice had access to regular chow and water ad libitum. Two- to five-month male $K8^{+/+}$, $K8^{+/-}$, and $K8^{-/-}$ mice and 4- to 7-mo-old male and female $K8^{flox/flox}$ and $K8^{flox/flox}$;Villin-Cre mice were used in this study.

Collection of Mouse Colonocytes

After the mouse was euthanized by CO_2 inhalation, the mouse colon was excised and rinsed with ice-cold PBS, and, if possible, any stool was flushed out using ice-cold PBS. The colon was then cut open longitudinally on an ice-cold glass plate, and any remaining stool or debris was removed using forceps and by rinsing with ice-cold PBS. Colon epithelium was collected by scraping the luminal side of the colon with an ice-cold microscope slide. These in vivo samples were used for SDS-PAGE and immunoblotting and are referred to as mouse colonocytes in this study.

SDS-PAGE and Immunoblotting

Samples of mouse colonocytes isolated from the colon epithelium were suspended in ice-cold homogenization buffer (0.187 M Tris·HCl pH 6.8, 3% SDS, and 5 mM EDTA) containing 1× complete protease inhibitor (PI) cocktail (Roche, Basel, Switzerland) and 1 mM phenylmethylsulfonyl fluoride in Potter-Elvehjem tissue homogenizers and homogenized by applying 75 strokes. Cell samples were collected in ice-cold homogenization buffer containing 1× PI cocktail and 1 mM phenylmethylsulfonyl fluoride. The samples were incubated at 95°C for 5 min and sheared with a 27-gauge needle. A Pierce BCA protein assay kit (Thermo Fisher Scientific, Waltham, MA) was used to determine sample protein concentrations, and the samples were normalized to a 5-μg protein/10-μL sample using 3× Laemmli sample buffer (30% glycerol, 3% SDS, 0.1875 M Tris·HCl pH 6.8, 0.015% bromophenol blue, and 3% β-mercaptoethanol). The samples were separated on 6 to 12% polyacrylamide gels using SDS-PAGE, transferred to polyvinylidene fluoride membranes, and analyzed by immunoblotting. Primary antibodies used for immunoblotting (1:1,000 dilution unless otherwise specified) were rabbit anti-β-actin (4967; Cell Signaling Technology, Danvers, MA), rat anti-Hsc70 (ADI-SPA-815; Enzo Life Sciences, Farmingdale, NY), rat anti-K8 (TROMA-I; Developmental Studies Hybridoma Bank, Iowa City, IA), rabbit anti-mitochondrial calcium uniporter (MCU; HPA016480; Sigma-Aldrich, St. Louis, MO), mouse MitoProfile Total Oxphos human WB antibody cocktail (1:200; ab110411; Abcam, Cambridge, UK), rabbit anti-mitofusin-2 (ab124773; Abcam), rabbit anti-mitofusin-2 (M6319; Sigma-Aldrich), rabbit anti-prohibitin (ab28172; Abcam), rabbit anti-trichoplein (1:500; orb100712; Biorbyt, Cambridge,

UK), and mouse anti-voltage-dependent anion channel (VDAC; MABN504; Sigma-Aldrich). Secondary antibodies used for immunoblotting (1:10,000 dilution) were anti-rabbit Alexa Fluor 800 (A32735; Thermo Fisher Scientific), anti-rabbit IgG-horseradish peroxidase (HRP) (W401B; Promega), anti-rat Alexa Fluor 488 (A-21208; Thermo Fisher Scientific), anti-rat Alexa Fluor 680 (A-21096; Thermo Fisher Scientific), anti-rat IgG-HRP (NA935; Cytiva), anti-rat IgG-HRP (7077; Cell Signaling Technology), and anti-mouse IgG-HRP (NA931; Cytiva). HRP signals were detected using Amersham ECL Western Blotting Detection Reagent (Cytiva) or ECL plus (PerkinElmer, Waltham, MA) and visualized on SUPER RX X-ray films (Fuji Corporation, Tokyo, Japan) or using iBright CL1000 or iBright FL1000 imaging systems (Thermo Fisher Scientific). Fluorescence signals were captured using an iBright FL1000 imaging system (Thermo Fisher Scientific). The immunoblotting results were quantified using ImageJ software (National Institutes of Health, Bethesda, MD) and normalized to loading controls (β-actin or Hsc70) using Microsoft Excel software (Microsoft, Redmond, WA).

Cell Culture and DNA Transfection

Human epithelial colorectal adenocarcinoma Caco-2 cells (HTB-37; ATCC, Manassas, VA) were used by our group to generate $K8^{+/+}$ and $K8^{-/-}$ Caco-2 cells using CRISPR/Cas9 technology (6, 18). $K8^{+/+}$ and $K8^{-/-}$ Caco-2 cells were grown in Dulbecco's modified Eagle's medium (DMEM) supplemented with 20% fetal calf serum (FCS), 2 mM L-glutamine, and 100 units/mL penicillin, and 100 μg/mL streptomycin. The cells were grown at 37°C in a 5% CO_2 atmosphere. For DNA transfection, ∼60% confluent $K8^{-/-}$ Caco-2 cells in 24-well plates were transfected with pcDNA or plasmids encoding human K8 (a kind gift from M Bishr Omary; Addgene plasmid no. 14742) and K18 (a kind gift from M Bishr Omary; Addgene plasmid no. 14741) using Lipofectamine 2000 (Thermo Fisher Scientific) according to the manufacturer's instructions; 1.75 μL Lipofectamine 2000 and 0.5 μg pcDNA plasmid or 0.25 μg K8 and 0.25 μg K18 plasmid DNA were used per well. Samples for Western blot analysis were prepared 72 h posttransfection.

Mitochondrial Respiration and Glycolysis Assays

Mitochondrial respiration [oxygen consumption rate (OCR)] and glycolytic rate (glycolytic proton efflux rate) were measured using a Seahorse XFe96 analyzer (Agilent, Santa Clara, CA) according to the manufacturer's instructions. All assay reagents were from Agilent. Briefly, 14–16 h before the assay, 15,000–40,000 $K8^{+/+}$ or $K8^{-/-}$ Caco-2 cells were seeded per well on a 96-well XF96 cell culture microplate (Agilent), and a XFe96 sensor cartridge (Agilent) was hydrated. On the day of the assay, the cells were washed twice and incubated with XF assay medium (XF DMEM medium pH 7.4 supplemented with 1 mM pyruvate, 2 mM glutamine, and 10 mM glucose) for 1 h in a 37°C non-CO_2 incubator. Mitochondrial respiration was assessed using the Seahorse XF Cell Mito Stress Test Kit according to the manufacturer's instructions. During the assay, the OCR of the cells was measured at baseline conditions and after modulation of mitochondrial respiration by the sequential addition of 1 μM oligomycin, 1 μM carbonyl cyanide-4 (trifluoromethoxy) phenylhydrazone (FCCP), and 0.5 μM rotenone/antimycin A. Glycolysis (glycolytic proton efflux rate) was measured using the Seahorse XF Glycolytic Rate Assay Kit according to the manufacturer's instructions. The results were normalized to total protein quantity measured by BCA protein assay, and the data were exported to and analyzed with the Seahorse XF Cell Mito Stress Test Report Generator or Agilent Seahorse Analytics.

Tetramethylrhodamine Ethyl Ester ΔΨm Plate Reader Assay

ΔΨm was measured using the tetramethylrhodamine ethyl ester (TMRE) probe (Abcam) according to the manufacturer's instructions. Briefly, 60,000 $K8^{+/+}$ or $K8^{-/-}$ Caco-2 cells were plated per well in a 96-well plate. The following day, the cells were incubated with 1,000 nM TMRE in FluoroBrite DMEM medium (Thermo Fisher Scientific) supplemented with 10% FCS, 2 mM L-glutamine, and 100 units/mL penicillin, and 100 μg/mL streptomycin for 20 min in a 37°C incubator. Postincubation, the TMRE solution was aspirated, and FluoroBrite medium was added to the sample wells. TMRE fluorescence was measured with a Hidex Sense microplate reader (Hidex, Turku, Finland) with the following settings: 544 nm with a 20-nm bandwidth for excitation, 616 nm with 8.5 nm for emission, and bottom read mode with 15 flashes. Background fluorescence values (wells containing cells and medium, but no dye) were subtracted from the results.

TMRE ΔΨm Flow Cytometry Assay

$K8^{+/+}$ or $K8^{-/-}$ Caco-2 cells were grown on standard six-well plates until 70–80% confluent. Before staining, the cells were washed with PBS, and FCCP-positive control cells were incubated with 50 μM FCCP for 10 min. TMRE cells and FCCP control cells were then stained with 150 nM TMRE for 1 h in a 37°C incubator, whereafter the TMRE-containing medium was aspirated, and the cells were washed with PBS. The cells were trypsinized, moved to Eppendorf tubes with DMEM, and centrifuged at 1,000 rpm for 10 min. The supernatant was discarded, and excess TMRE was removed by three cycles of washing with PBS and centrifugation (1,000 rpm for 5–10 min). Finally, the cell pellets were resuspended in 1–2 mL of PBS and filtered. The flow cytometry experiment was conducted with a BD LSR II (BD Biosciences, Franklin Lakes, NJ) and analyzed with Flowing software 2.5.1 (Cell Imaging and Cytometry Core, Turku Bioscience Center, Turku, Finland). Unstained samples were used to measure the background signal, which was used to normalize the fluorescence values of the TMRE-stained samples.

Ca^{2+} Measurements

Cytoplasmic and mitochondrial Ca^{2+} measurements in $K8^{+/+}$ and $K8^{-/-}$ Caco-2 cells were performed using the Ca^{2+} probe aequorin targeted to the cytoplasm (nontarget aequorin; cyto-Aeq; a kind gift from Professor Paolo Pinton, University of Ferrara, Ferrara, Italy) and mitochondrial matrix (aequorin fused with the mitochondrial presequence of subunit VIII of cytochrome c oxidase; mito-Aeq; a kind gift from Professor Paolo Pinton), respectively (35). Briefly, 15,000–20,000 $K8^{+/+}$ or $K8^{-/-}$ Caco-2 cells were seeded per well on a 96-well plate. The day after, the cells were

transfected with cyto-Aeq or mito-Aeq plasmid DNA using Lipofectamine 2000 (Thermo Fisher Scientific) according to the manufacturer's instructions; 0.1 μg plasmid DNA and 0.35 μL Lipofectamine 2000 were used per well. Twenty-four hours posttransfection, the cells were washed three times with HEPES-buffered saline solution (HBSS buffer: 118 mM NaCl, 4.6 mM KCl, 10 mM glucose, and 20 mM HEPES, pH 7.4) supplemented with 1 mM $CaCl_2$ and incubated in HBSS containing 5 μM wild-type coelenterazine (Synchem, Elk Grove Village, IL) and 1 mM $CaCl_2$ for 1 h in room temperature and darkness. Postincubation, the Hidex microplate reader was used to record aequorin-generated luminescence. Briefly, baseline luminescence (resting Ca^{2+}) was recorded for 10 s, after which Ca^{2+} signaling was activated by the addition of 100 μM ATP. When no further changes in luminescence were observed, the cells were permeabilized with HBSS containing 100 μM digitonin (Sigma-Aldrich) and 10 mM Ca^{2+}, and maximum luminescence values were recorded for calibration of the results. The acquired aequorin luminescence values were calibrated into the Ca^{2+} concentration ($[Ca^{2+}]$) values using a previously described formula (35).

Mitochondrial Motility Assay

$K8^{+/+}$ and $K8^{-/-}$ Caco-2 cells were plated on glass bottom microwell dishes (MatTek Corporation, Ashland, MA). On the next day, the cells were washed two times with FluoroBrite DMEM, and the cells were incubated with 50 nM TMRE or 250 nM MitoTracker Deep Red (Thermo Fisher Scientific) in FluoroBrite DMEM for 30 min in a 37°C incubator. Postincubation, the TMRE- or MitoTracker Deep Red-containing medium was replaced with fresh FluoroBrite DMEM, and the cells were imaged with a SP5 matrix confocal microscope (Leica, Wetzlar, Germany) with a heated incubator stage (37°C and 5% CO_2). The cells were imaged every 10 s for 2 min to track the movements of mitochondria. Mitochondrial movement was quantified using the manual tracking plugin in Fiji software (36). Ten to fifteen mitochondria per image were tracked, and in total, the motility of 92–208 mitochondria per genotype was analyzed. Fiji calculates the velocity and distance traveled by each mitochondrion at every time point, and the average velocity and distance traveled by every mitochondrion were determined.

Transmission Electron Microscopy Analysis

Transmission electron microscopy (TEM) samples of $K8^{+/+}$ and $K8^{-/-}$ mouse proximal colon tissue were prepared as previously described (22), and TEM images of colonocytes in the upper regions of crypts and surface epithelium were captured with a JEM-1400 Plus transmission electron microscope (Jeol, Peabody, MA). The images were randomized and blinded for mitochondrial morphology analysis using Fiji software. Mitochondrial area was determined by drawing a region of interest around mitochondria and calculating the resulting area. Mitochondrial shape was classified as long, oval, or round, and the shape of mitochondria was assessed by measuring the aspect ratio (AR) of mitochondria. Mitochondria were classified as long if mitochondrial length was two times larger than the width (AR: ≥2), oval if mitochondrial length was from one and a half times up to two times larger than the width (AR: 1.5–2), and round if mitochondrial length was less than one and a half times larger than the width (AR: ≤1.5).

Statistical Analysis

The results were statistically analyzed with a *t* test where applicable using Prism 9 (GraphPad Software, San Diego, CA). The results show the mean ± SD with significant differences shown as $P < 0.05$, $P < 0.01$, or $P < 0.001$.

RESULTS

K8 Maintains Mitochondrial Shape In Vivo in Colonocytes

As colonocytes devoid of K8 in our previous study showed fewer mitochondrial cristae (22), we investigated whether other changes in mitochondrial shape are manifested in colonocytes of $K8^{-/-}$ mice. Ultrastructural analysis of $K8^{+/+}$ and $K8^{-/-}$ colonocytes in vivo using TEM revealed that ∼46% of $K8^{+/+}$ colonocyte mitochondria are round, while ∼28% are long and ∼26% are oval (Fig. 1, *A* and *B*). In contrast, loss of K8 elicited a shift in mitochondrial shape, as $K8^{-/-}$ colonocytes displayed significantly fewer mitochondria that have a long (∼9%) or oval (∼15%) shape and an increased number of round-shaped mitochondria (∼76%) compared with $K8^{+/+}$ colonocytes (Fig. 1*B*). In addition, a significant 28% decrease in average mitochondrial area was observed in $K8^{-/-}$ colonocytes (0.19 μm^2) in comparison to $K8^{+/+}$ colonocytes (0.26 μm^2; Fig. 1*C*), while there was no difference in the number of mitochondria (Fig. 1*D*). Taken together, these results indicate that K8 is important for maintaining mitochondrial shape and size in colonocytes.

Mitochondrial Motility Is Increased in Caco-2 Cells Lacking K8

To gain insight into the impact of K8 on mitochondrial physiological processes in colonocytes, we next performed in vitro-based functional assays on $K8^{+/+}$ and $K8^{-/-}$ Caco-2 colon cancer cells. To assess whether K8 is involved in the regulation of mitochondrial motility in colonocytes, we tracked mitochondrial movement in $K8^{+/+}$ and $K8^{-/-}$ Caco-2 cells labeled with TMRE or MitoTracker Deep Red (Fig. 2*A*). Compared with $K8^{+/+}$ Caco-2 cells, mitochondrial velocity in cells lacking K8 increased by ∼39% as seen by TMRE (Fig. 2*B*) and by ∼31% as seen by MitoTracker Deep Red (Fig. 2*C*). Similarly, the average distance traveled during 2 min was ∼40% longer as seen by TMRE and ∼31% longer as seen by MitoTracker Deep Red. While there are minor discrepancies in the actual velocity and distance traveled of TMRE- and MitoTracker Deep Red-stained mitochondria, the results obtained with both dyes indicate that mitochondrial movements are restrained by keratins.

Mitochondrial Respiration and ΔΨm Are Diminished in $K8^{-/-}$ Caco-2 Cells

To elucidate if mitochondrial oxidative phosphorylation and ATP production are affected in colon epithelial cells lacking K8, we compared mitochondrial respiration in $K8^{+/+}$ and $K8^{-/-}$ Caco-2 cells using the Seahorse XF Cell Mito Stress Test Kit (Fig. 3*A*). Compared with wild-type cells, $K8^{-/-}$ cells exhibited decreased basal respiration, ATP

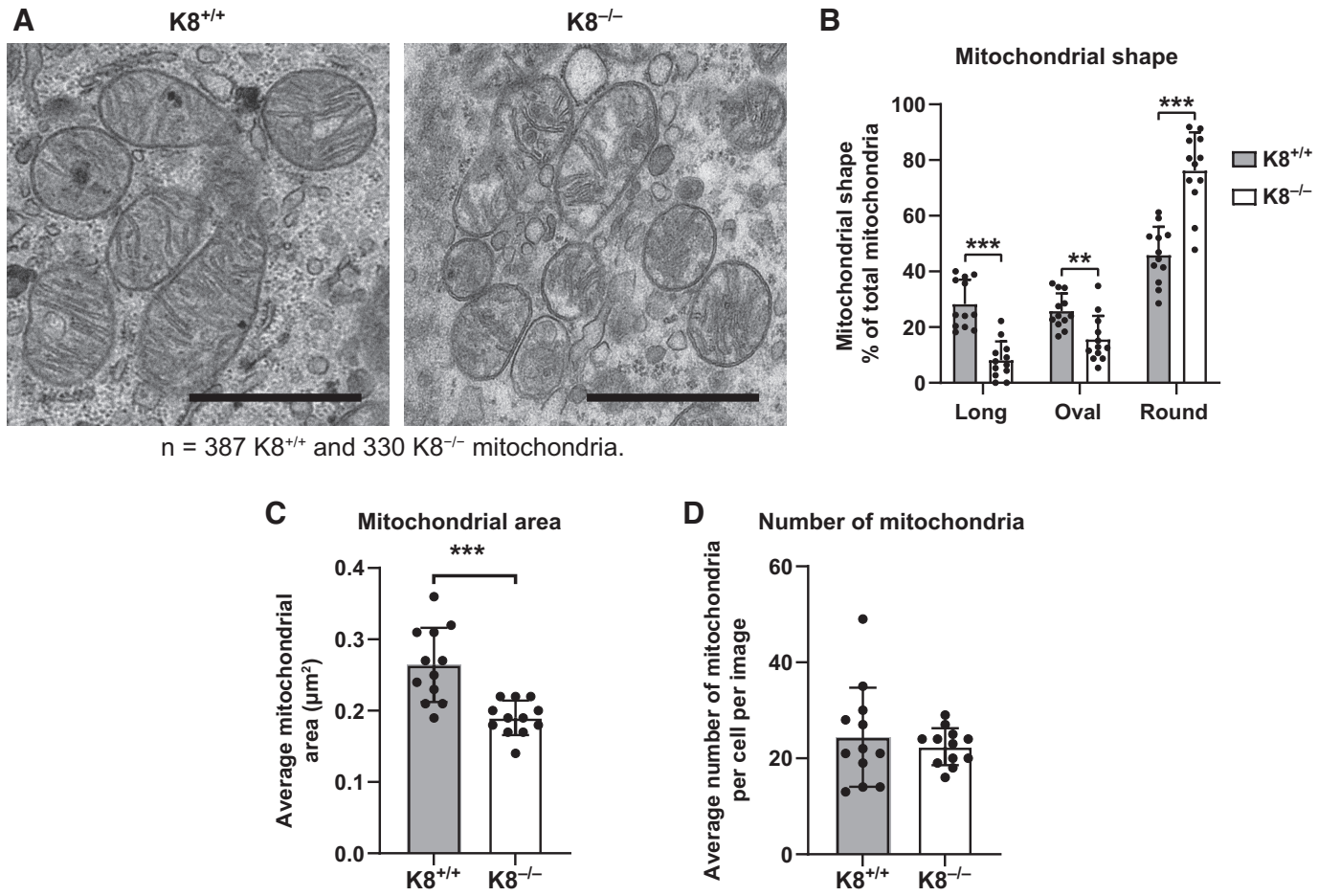

Figure 1. K8$^{-/-}$ mouse colonocytes display smaller and more round mitochondria. Mitochondrial morphology was assessed by transmission electron microscopy (TEM) imaging of colonocytes in the surface epithelium and the upper regions of crypts in K8$^{+/+}$ and K8$^{-/-}$ mouse proximal colon tissue samples. *A*: representative TEM images of K8$^{+/+}$ and K8$^{-/-}$ mouse colonocytes. Scale bar = 1 μm. *B*: the shape of K8$^{+/+}$ and K8$^{-/-}$ colonocyte mitochondria was determined and is displayed as the percentage of long, oval, or round mitochondria of total mitochondria. *C* and *D*: analysis of mitochondria area (*C*) and the number of mitochondria (*D*) in K8$^{+/+}$ and K8$^{-/-}$ colon tissue TEM images. The results represent the average ($n = 6$ images/mouse, 2 mice/genotype; 387 K8$^{+/+}$ and 330 K8$^{-/-}$ mitochondria analyzed) ± SD with significant differences shown: $^{**}P < 0.01$ and $^{***}P < 0.001$.

production, maximal respiration, and spare respiratory capacity, while proton leak and nonmitochondrial oxygen consumption were comparable to K8$^{+/+}$ (Fig. 3, *B–G*). During oxidative phosphorylation, proton pumps in the inner mitochondrial membrane (IMM) generate ΔΨm. As ΔΨm is tightly linked to and essential for mitochondrial respiration, we measured it using the fluorescent dye TMRE, which is sensitive to changes in ΔΨm. As seen by both flow cytometry and plate reader assays, ΔΨm was significantly diminished, on average, by 30–50% in K8$^{-/-}$ cells compared with wild-type cells (Fig. 4, *A* and *B*). The ionophore FCCP, which depolarizes the mitochondrial membrane and is used as a positive control in this assay, efficiently reduced K8$^{+/+}$ ΔΨm, while the reduction was much smaller from the already low ΔΨm in K8$^{-/-}$ cells. Intriguingly, as seen in the flow cytometry assays, ΔΨm in untreated K8$^{-/-}$ cells decreased almost to a similar level as in FCCP-treated K8$^{+/+}$ and K8$^{-/-}$ cells, while the decrease in the plate reader assays was not as extensive (Fig. 4, *A* and *B*). K8$^{-/-}$ mitochondria are thus more depolarized and/or inactive than K8$^{+/+}$ mitochondria, indicating that K8 is important for maintaining ΔΨm in colonocytes. To address whether another major source of cellular energy, glycolysis, is affected in K8-deficient cells, we measured glycolytic flux in K8$^{+/+}$ and K8$^{-/-}$ Caco-2 cells. Seahorse analysis of glycolytic proton efflux rate revealed that basal glycolysis is unaltered upon K8 loss (Fig. 3*H*), indicating that glycolysis does not compensate for the decreased mitochondrial respiration. Taken together, these results suggest that K8 is a key player in mitochondrial bioenergetics in colonocytes.

Mitochondrial Proteins Associated with Oxidative Phosphorylation and Mitochondrial Function Are Downregulated in K8$^{-/-}$ Colonocytes

Mitochondrial respiration and ΔΨm are linked to the protein levels and activity of oxidative phosphorylation complex proteins, and a partial or complete loss of cristae has been associated with decreased mitochondrial bioenergetics. As K8$^{-/-}$ colonocytes exhibit fewer mitochondrial cristae (22) and K8$^{-/-}$ Caco-2 cells exhibit diminished respiration and ΔΨm, we assessed the levels of oxidative phosphorylation complex proteins in K8$^{+/+}$ cells and K8$^{-/-}$ Caco-2 cells by immunoblotting. Significantly decreased protein levels of

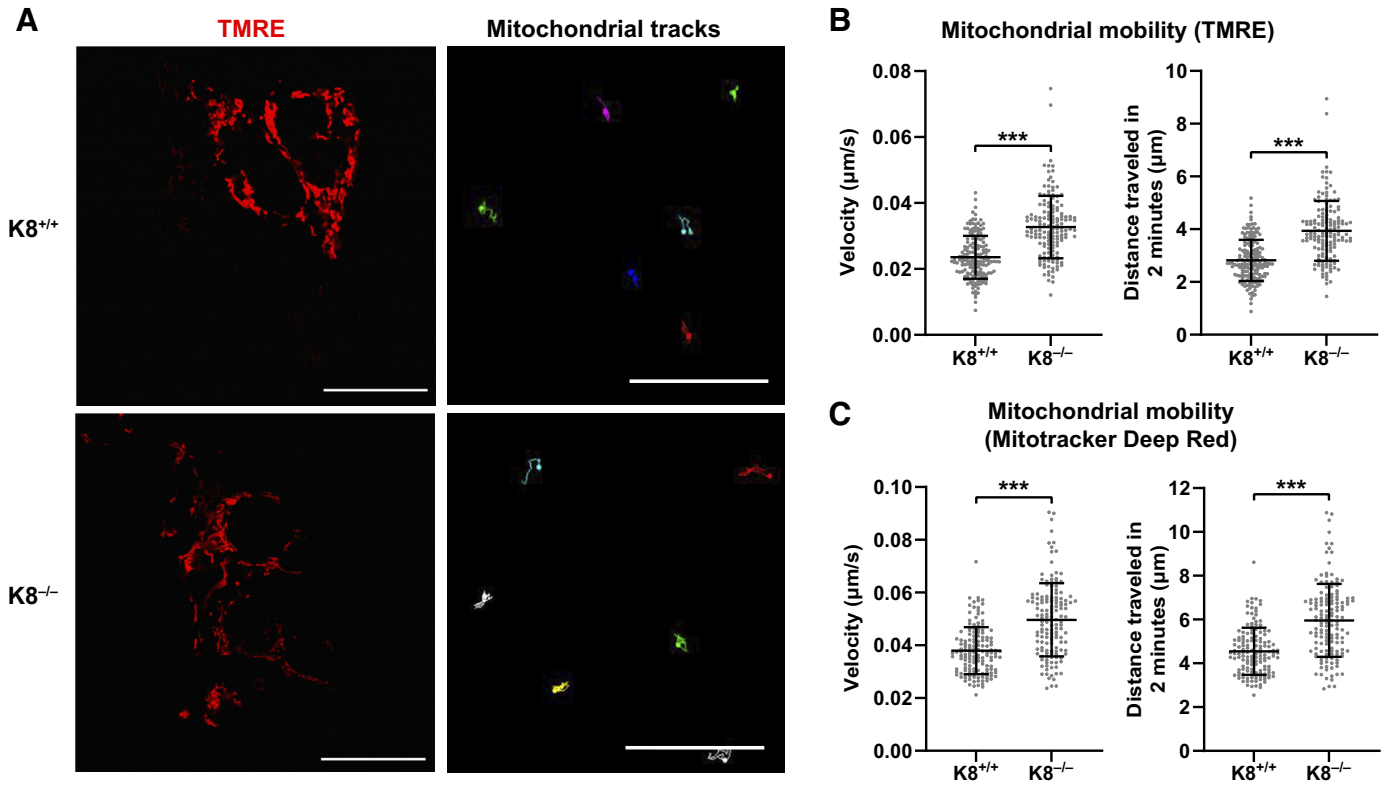

Figure 2. Mitochondrial motility is increased in Caco-2 cells lacking K8. $K8^{+/+}$ and $K8^{-/-}$ Caco-2 cells were stained with mitochondrial dyes tetramethylrhodamine ethyl ester (TMRE) or MitoTracker Deep Red and tracked by confocal microscopy. *A*: representative images of total mitochondrial tracks (*left*: red color; scale bars = 25 μm) and individual mitochondrial tracks (*right*: various colors; scale bars = 12.5 μm) in TMRE-stained $K8^{+/+}$ and $K8^{-/-}$ Caco-2 cells. The tracks represent the movement of mitochondria over a 2-minute time lapse. *B* and *C*: velocities of mitochondria stained with TMRE (*B*) and MitoTracker Deep Red (*C*) were quantified. The results represent the average (n = 149–165 mitochondria/genotype for TMRE; n = 145 mitochondria/genotype for MitoTracker Deep Red; small dots represent individual values) ± SD with significant differences shown: ***$P < 0.001$.

complex I (subunit NDUFB8) and complex IV (subunit COX II) were observed in $K8^{-/-}$ cells, while the levels of complex III (subunit UQCRC2) and complex V (subunit ATP5A) were comparable to $K8^{+/+}$ cells (Fig. 5, *A–E*). To elucidate if a similar phenotype is observed in vivo in noncancer cells, we determined mouse colonocyte oxidative phosphorylation complex levels and found that $K8^{-/-}$ mouse colonocytes exhibit decreased levels of complexes I, III, IV, and V (Fig. 6, *A–E*). In addition, the protein levels of complex III and V were decreased in $K8^{+/-}$ colonocytes; however, the decrease was intermediate compared with $K8^{-/-}$ (Fig. 6, *A–C*).

As oxidative phosphorylation complex protein levels are decreased in $K8^{-/-}$ Caco-2 cells, we analyzed the protein levels of the mitochondrial regulatory proteins mitofusin-2 and prohibitin, which are involved in the regulation of oxidative phosphorylation complex protein expression, stability, and activity (37–40). Mitofusin-2 and prohibitin protein levels were significantly decreased both in vitro in $K8^{-/-}$ Caco-2 cells and in vivo in $K8^{-/-}$ mouse colonocytes compared with their wild-type counterparts, while no change was observed in $K8^{+/-}$ colonocytes (Fig. 5, *F* and *G*, and Fig. 6, *F* and *G*). Additionally, the protein levels of trichoplein, which may facilitate keratin-mitochondria interactions, were unaltered in both $K8^{-/-}$ Caco-2 cells and $K8^{+/-}$ and $K8^{-/-}$ mouse colonocytes (Figs. 5*H* and 6*H*). As mitofusin-2, in addition to its role in respiration, is important for mitochondrial dynamics (25), which are altered in $K8^{-/-}$ colonocytes (Fig. 1), we tested whether mitofusin-2 levels are dependent on K8 levels. Reintroduction of K8 and its partner K18 into $K8^{-/-}$ Caco-2 cells led to a significant increase in mitofusin-2 levels compared with control $K8^{-/-}$ Caco-2 cells, indicating that the K8 loss-associated mitochondrial phenotype could be mediated through mitofusin-2 (Fig. 5, *I–K*). The downregulation of these oxidative phosphorylation complex proteins and mitochondrial regulatory proteins may contribute to the decreased mitochondrial respiration and $\Delta\Psi m$ in $K8^{-/-}$ cells.

Mitochondrial Ca^{2+} Dynamics Are Altered and Ca^{2+} Levels Are Decreased in $K8^{-/-}$ Caco-2 Cells

As mitochondria are major Ca^{2+} signaling hubs and Ca^{2+} stimulates respiration (41, 42), we studied mitochondrial Ca^{2+} dynamics in vitro in $K8^{+/+}$ and $K8^{-/-}$ Caco-2 cells using the Ca^{2+} probe aequorin targeted to the mitochondrial matrix. Upon stimulation of Ca^{2+} signaling, both $K8^{+/+}$ and $K8^{-/-}$ cells exhibited a mitochondrial Ca^{2+} response; however, Ca^{2+} dynamics were altered in $K8^{-/-}$ cells (Fig. 7*A*). In particular, K8 absence elicited a small, short-lived Ca^{2+} peak immediately upon stimulation of mitochondrial Ca^{2+} signaling (Fig. 7*A*). In addition, the mitochondrial Ca^{2+} levels were decreased as seen by Δ mitochondrial $[Ca^{2+}]$ (the difference between maximum and minimum) and area under the curve (AUC) mitochondrial $[Ca^{2+}]$ values (Fig. 7, *B* and *C*). Analysis of cytoplasmic Ca^{2+} using nontargeted aequorin revealed a similar, albeit

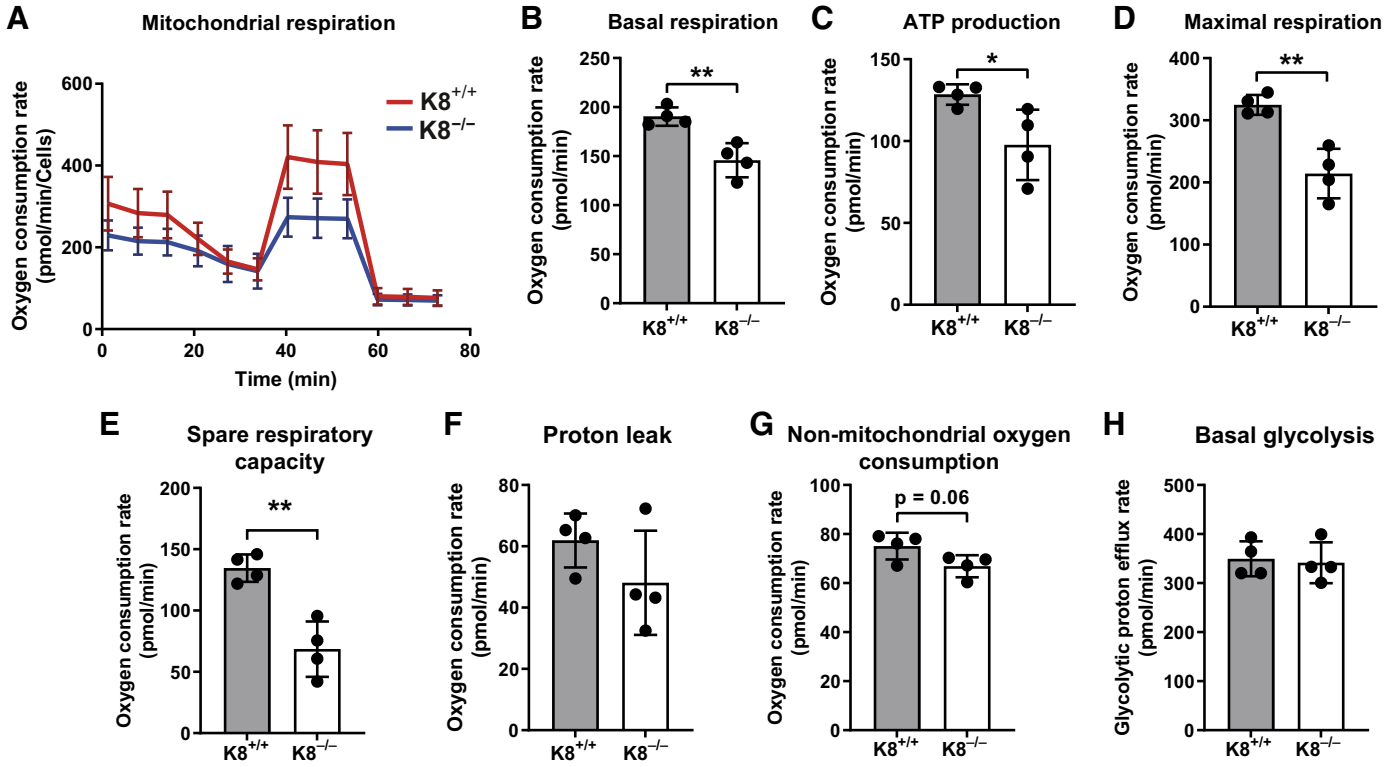

Figure 3. Mitochondrial respiration and respiratory capacity, but not glycolysis, are diminished in K8$^{-/-}$ Caco-2 cells. *A*: Seahorse XF Cell Mito Stress Test Kit was used to measure the oxygen consumption rates of K8$^{+/+}$ and K8$^{-/-}$ Caco-2 cells, and the results were normalized to total protein quantity. *B–G*: Seahorse XF Mito Stress Test Report Generator was used to calculate basal respiration (*B*), ATP production (*C*), maximal respiration (*D*), spare respiratory capacity (*E*), proton leak (*F*), and nonmitochondrial oxygen consumption (*G*). *H*: Seahorse XF Glycolytic Rate Assay Kit was used to measure the glycolytic proton efflux rate of K8$^{+/+}$ and K8$^{-/-}$ Caco-2 cells, and the results were normalized to total protein quantity. Agilent Seahorse Analytics was used to calculate basal glycolysis. The results represent the average oxygen consumption rate/glycolytic proton efflux rate (n = 4/genotype, with 5–6 technical replicates each) ± SD with significant differences shown: *$P < 0.05$ and **$P < 0.01$.

smaller, outcome with altered cytoplasmic Ca^{2+} dynamics and decreased AUC but no change in Δ for cytoplasmic [Ca^{2+}] (Fig. 7, *D–F*), indicating that K8 may also affect cytoplasmic Ca^{2+} signaling in addition to mitochondrial Ca^{2+} regulation. Analysis of the major mitochondrial Ca^{2+} transporters, the outer mitochondrial membrane (OMM) Ca^{2+} transporter VDAC and the IMM Ca^{2+} transporter MCU, revealed unaltered protein levels of VDAC and MCU in K8$^{-/-}$ Caco-2 cells (Fig. 7, *G–I*). In contrast, VDAC and MCU protein levels were decreased in vivo in K8$^{-/-}$ mouse colonocytes compared with K8$^{+/+}$, while no change was observed in K8$^{+/-}$ (Fig. 7, *J–L*). These results suggest that an attenuated mitochondrial Ca^{2+} response may contribute to the energy metabolism phenotype in K8$^{-/-}$ Caco-2 cells.

To assess whether the mitochondrial phenotype observed in vitro in K8$^{-/-}$ Caco-2 cells and in vivo in colonocytes of full-body K8$^{-/-}$ mice is colonocyte autonomous, we assessed the protein levels of mitochondrial Ca^{2+} transporters VDAC and MCU and the mitochondrial regulatory proteins prohibitin and mitofusin-2 in K8$^{flox/flox}$;Villin-Cre mice, in which K8 is absent specifically in intestinal epithelial cells (15). Compared with K8$^{flox/flox}$ mice, the protein levels of VDAC, MCU, and mitofusin-2 were decreased in K8$^{flox/flox}$;Villin-Cre mouse colonocytes, while no difference was seen for prohibitin (Fig. 7, *M–Q*). These findings indicate that the mitochondrial phenotype in K8$^{-/-}$ colonocytes is colonocyte autonomous.

DISCUSSION

In this work, we have characterized the impact of simple epithelial keratins on mitochondrial homeostasis and energy metabolism in colonocytes (summarized in Fig. 8). Our results show that mitochondria are smaller and rounder in vivo in K8$^{-/-}$ mouse colonocytes and that K8 loss in vitro in Caco-2 cells correlates with increased mitochondrial motility. K8$^{-/-}$ Caco-2 cells further display diminished mitochondrial respiration and decreased ΔΨm, whereas glycolysis is unaffected. Oxidative phosphorylation complex, prohibitin, and mitofusin-2 protein levels are reduced both in vivo in mouse colonocytes and in vitro in Caco-2 cells lacking K8. Furthermore, we show that mitofusin-2 levels could be rescued by reexpression of K8/K18 in Caco-2 cells lacking K8, suggesting that the impact of keratins on mitochondria may at least partly be mediated through mitofusin-2 in colonocytes. Importantly, we also observed decreased Ca^{2+} levels and altered Ca^{2+} dynamics in K8$^{-/-}$ Caco-2 cell mitochondria and cytoplasm, indicating that K8 is important for the dynamic control of Ca^{2+} in colonocytes. The protein levels of mitochondrial Ca^{2+} transporters VDAC and MCU were unaltered in K8$^{-/-}$ Caco-2 cells, while they were downregulated in K8$^{-/-}$ mouse colonocytes. Finally, reduced protein levels of mitofusin-2, VDAC, and MCU were observed in colonocytes from K8$^{flox/flox}$;Villin-Cre mice with intestinal-specific ablation of K8, indicating that the K8$^{-/-}$ mitochondrial

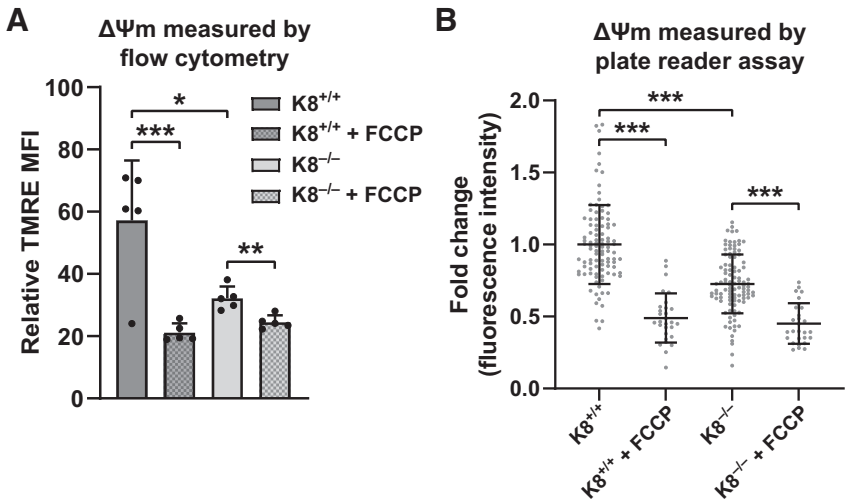

Figure 4. Loss of K8 leads to decreased mitochondrial membrane potential (ΔΨm) in Caco-2 cells. *A* and *B*: ΔΨm was assessed in $K8^{+/+}$ and $K8^{-/-}$ Caco-2 cells using the ΔΨm-sensitive probe tetramethylrhodamine ethyl ester (TMRE). FCCP, which causes mitochondrial depolarization and decreases ΔΨm, was used as a positive control. *A*: TMRE fluorescence intensity levels analyzed by flow cytometry. The measured median fluorescence intensity (MFI) values were normalized to the MFI of unstained cells. The results represent the average relative MFI ($n = 5$ replicate assays/genotype, with 50,000–100,000 cells/assay) ± SD with significant differences shown: $^{*}P < 0.05$, $^{**}P < 0.01$, and $^{***}P < 0.001$. *B*: TMRE fluorescence intensity levels analyzed by plate reader assay. The measured fluorescence intensity values were corrected for the background signal in unstained controls. The results represent the average ($n = 4$, with 5–29 technical replicates each per genotype and condition/assay; small dots represent individual values) fold change in TMRE fluorescence intensity relative to $K8^{+/+}$ ± SD with significant differences shown: $^{***}P < 0.001$.

energy metabolism likely is colonocyte autonomous. Our findings in these three different in vivo and in vitro $K8^{-/-}$ model systems attribute an important role for K8 in maintaining mitochondrial morphology, motility, energy metabolism, and Ca^{2+} homeostasis in colonocytes.

Mitochondria continuously adapt and respond to cellular cues through the regulation of mitochondrial dynamics, facilitating changes in mitochondrial shape, size, number, location, and tethering (24, 25). IFs and IF-associated proteins, including keratins, vimentin, desmin, neurofilaments, and plectin, are emerging as important regulators of mitochondrial dynamics and function in different organs and cell types (26, 27). Here, we observed in vivo in K8-deficient colon a shift in mitochondrial morphology from larger, elongated mitochondria to smaller and rounder mitochondria, which could be a consequence of the reduced levels of the mitochondrial fusion protein mitofusin-2 in $K8^{-/-}$ colonocytes (7, 43, 44). Furthermore, $K8^{-/-}$ colonocyte mitochondria display fewer cristae (22). Our observations in the colon are in agreement with earlier studies reporting similar phenotypes in $K8^{-/-}$ or K8 G62C or K18 R90C mutant mouse β-cells and/or hepatocytes (7, 28). Conversely, $K6a/K6b^{-/-}$ and $K5^{-/-}$ epidermal keratinocytes exhibit swollen mitochondria in conjunction with a partial or complete loss of cristae, while mitochondrial size and shape were unaffected (8, 32), suggesting that a phenotype with rounder and/or smaller mitochondria upon keratin loss or mutation is specific for simple epithelial keratin-expressing epithelia. Furthermore, IFs can tether mitochondria and modulate mitochondrial movement (26), and the loss or mutation of IFs has been linked to increased mitochondrial motility and/or disorganization of mitochondria (7, 8, 45, 46). Here, $K8^{-/-}$ Caco-2 cells display increased mitochondrial motility, which is in line with earlier observations in keratin-deficient β-cells and keratinocytes (7, 8). These findings by us and others support the notion that IFs in different cell types help anchor and confine mitochondria spatially (26, 27), which may contribute to local ATP production and Ca^{2+} buffering. Taken together, our findings support a role for K8 in maintaining mitochondrial size and shape and restraining mitochondrial movement in colonic epithelium.

$K8^{-/-}$ colonocytes exhibit a mitochondrial energy metabolism phenotype characterized by blunted ketogenesis (22). Here, we expand on this by showing that $K8^{-/-}$ Caco-2 cells exhibit diminished mitochondrial respiration. Furthermore, ΔΨm, a dynamic indicator of mitochondrial respiration, is significantly decreased in $K8^{-/-}$ cells. Interestingly, in contrast to $K8^{-/-}$ colonocytes, hepatocytes deficient for K8 do not exhibit a phenotype with reduced respiration or ketogenesis, indicating that K8 impacts mitochondrial metabolism differentially in colonocytes and hepatocytes (22, 28). Notably, glycolysis is unaffected by K8 loss in Caco-2 cells, indicating that it does not compensate for the decreased respiration in these cells. Similar energy metabolism phenotypes have been reported for other epithelial cell types that display IF mutations or lack IFs or plectin (7, 8, 31, 47–50). Conversely, mouse keratinocytes lacking all type I keratins display increased respiration, suggesting that keratins can also restrict mitochondrial activity (30). Several respiratory chain proteins are downregulated both in vivo in $K8^{-/-}$ colonocytes and in vitro in $K8^{-/-}$ Caco-2 cells, which, as $K8^{-/-}$ mouse colonocyte mitochondria display fewer cristae (22), could reflect insufficient IMM surface area for efficient oxidative phosphorylation complex assembly and activity (51, 52). Additionally, the decreased levels of complexes I and IV could possibly explain the diminished ΔΨm, as it is complexes I, III, and IV that generate ΔΨm by pumping protons across the IMM. The smaller, rounder, and more motile mitochondria of $K8^{-/-}$ colonocytes may also negatively affect energy metabolism, as respiration may be more efficient in large elongated

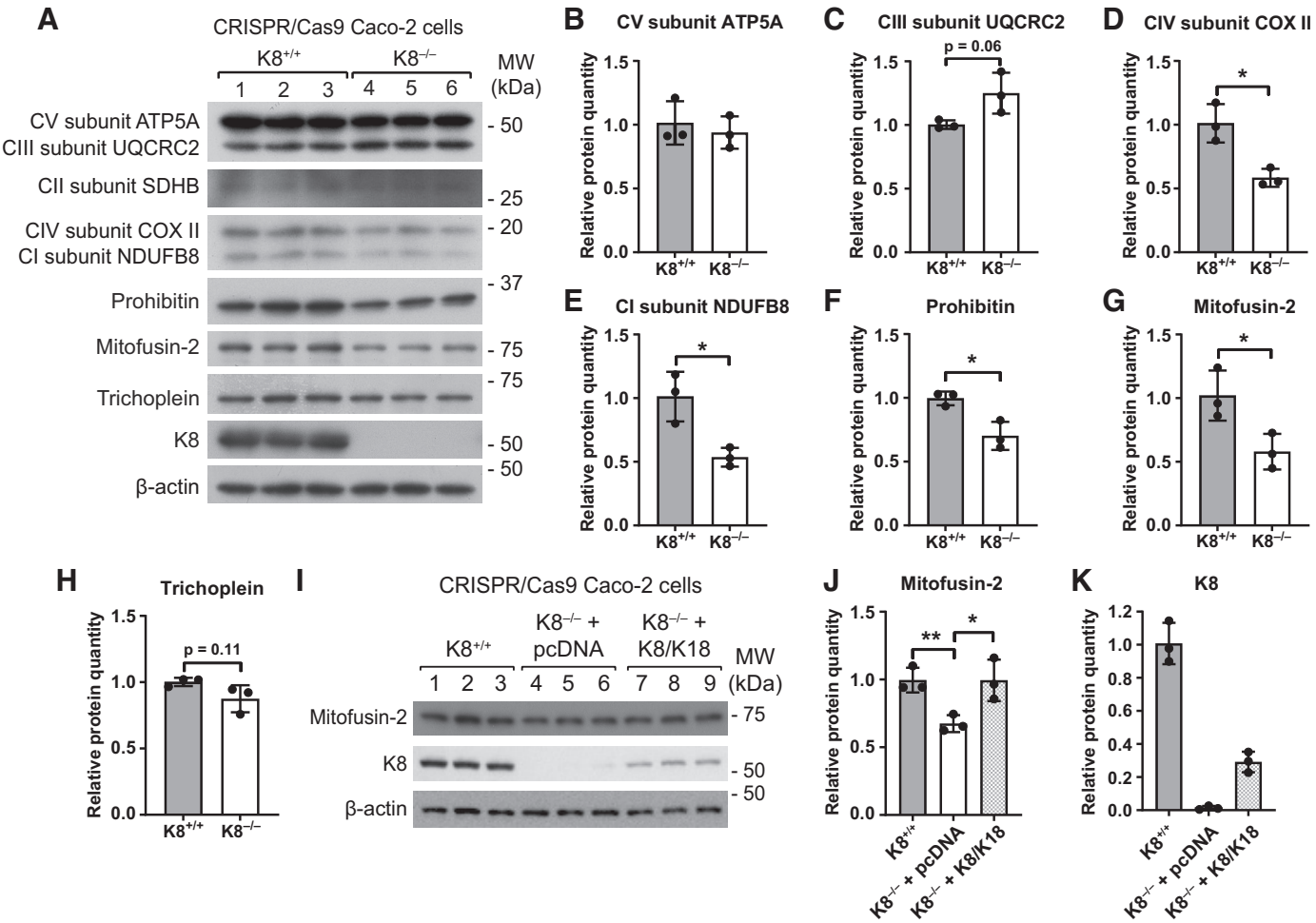

Figure 5. K8$^{-/-}$ Caco-2 cells exhibit decreased protein levels of oxidative phosphorylation complexes and mitochondrial regulatory proteins, and reintroduction of K8 rescues the downregulation of mitofusin-2. *A–H*: K8$^{+/+}$ and K8$^{-/-}$ Caco-2 cells were analyzed by immunoblotting (*A*) for oxidative phosphorylation protein complex V (CV) subunit ATP5A (*B*); complex III (CIII) subunit UQCRC2 (*C*); complex II (CII) subunit SDHB, complex IV (CIV) subunit COX II (*D*); and complex I (CI) subunit NDUFB8 (*E*) and mitochondrial regulatory proteins prohibitin (*F*), mitofusin-2 (*G*), and trichoplein (*H*). The K8 genotype is shown by the K8 blot (notably, the same K8 blot is presented in Fig. 7*G*, as the same sample set was used here). The immunoblots were quantified and normalized against β-actin. The results represent the average ($n = 3$/genotype) fold change relative to K8$^{+/+}$ ± SD, with significant differences shown: $^{*}P < 0.05$. *I–K*: K8$^{-/-}$ Caco-2 cells transfected with pcDNA or K8 and K18 DNA plasmids and K8$^{+/+}$ cells were analyzed by immunoblotting (*I*) for mitofusin-2 (*J*) and K8 (*K*). The immunoblots were quantified and normalized against β-actin. The results represent the average ($n = 3$/genotype) fold change relative to K8$^{+/+}$ ± SD, with significant differences shown for mitofusin-2: $^{*}P < 0.05$ and $^{**}P < 0.01$. MW (kDa) indicates the closest molecular mass marker on the Western blots.

mitochondria (25, 53, 54), and higher metabolic activity has been observed in less motile mitochondria (55).

The OMM protein mitofusin-2 can modulate mitochondrial metabolism independently of its function in mitochondrial dynamics (56), and mitofusin-2 deficiency has been associated with diminished respiration, decreased $\Delta\Psi m$, and decreased respiratory chain complex activity or protein levels (39, 40, 57). Similarly, the IMM protein prohibitin maintains mitochondrial respiration by stabilizing and stimulating respiratory chain complex activity, while, conversely, prohibitin deficiency leads to reduced respiratory chain activity (37, 58–60). Consequently, the mitofusin-2 and prohibitin deficiency in K8$^{-/-}$ colonocytes likely contributes to impaired respiration. Further, the decreased mitochondrial Ca^{2+} levels in K8$^{-/-}$ Caco-2 cells may contribute to the dysfunctional respiration, as mitochondrial Ca^{2+} uptake enhances respiration by stimulating the activity of TCA cycle and respiratory chain enzymes (41, 42). Notably, the observed changes in mitochondrial energy metabolism upon K8 loss are similar in vivo in mice colonocytes and in vitro in human colorectal cancer cells, suggesting a role for colonocyte keratins in mitochondrial metabolism in both humans and mice and in normal and disease states. However, further research is needed to elucidate the sequence of events leading to blunted mitochondrial respiration upon K8 loss. Further, given our present and prior findings (22), and that K8$^{-/-}$ mice display colonocyte hyperproliferation (16), another important question for future studies is how rapid proliferation can take place in these metabolically compromised colonocytes.

K8$^{-/-}$ Caco-2 cells display altered dynamics and decreased levels of mitochondrial matrix and cytoplasmic Ca^{2+}. Mitochondrial Ca^{2+} entry is facilitated by VDAC in the OMM and MCU in the IMM (41, 42). VDAC and MCU levels are unaltered in K8$^{-/-}$ Caco-2 cells, thus likely excluding a role for

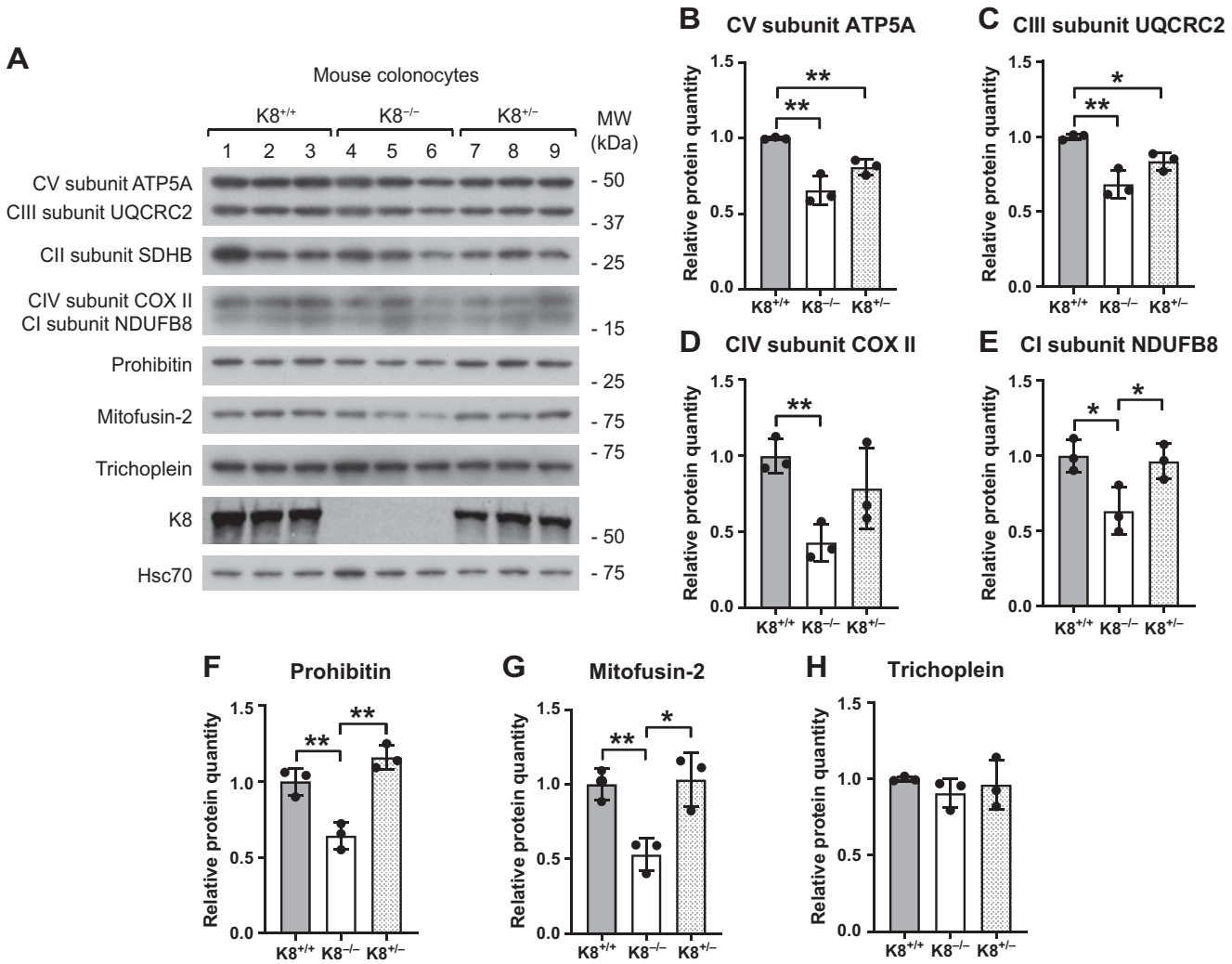

Figure 6. K8$^{-/-}$ mouse colonocytes display decreased protein levels of oxidative phosphorylation complexes and mitochondrial regulatory proteins. *A–H*: isolated colonocytes from K8$^{+/+}$, K8$^{-/-}$ and K8$^{+/-}$ mice were analyzed by immunoblotting (*A*) for oxidative phosphorylation protein complex V (CV) subunit ATP5A (*B*); complex III (CIII) subunit UQCRC2 (*C*); complex II (CII) subunit SDHB, complex IV (CIV) subunit COX II (*D*); and complex I (CI) subunit NDUFB8 (*E*) and mitochondrial regulatory proteins prohibitin (*F*), mitofusin-2 (*G*), and trichoplein (*H*). The K8 genotype is shown by the K8 blot (notably, the same K8 blot is presented in Fig. 7*J*, as the same sample set was used here). The immunoblots were quantified and normalized against Hsc70. The results represent the average ($n = 3$ male mice/genotype) fold change relative to K8$^{+/+}$ ± SD, with significant differences shown: $^{*}P < 0.05$ and $^{**}P < 0.01$. MW (kDa) indicates the closest molecular mass marker on the Western blots.

them in the observed phenotype. Conversely, VDAC and MCU are downregulated in K8$^{-/-}$ mouse colonocytes, indicating that mitochondrial Ca^{2+} uptake may be deficient also in vivo. It is unclear why VDAC and MCU levels are not similarly affected in cultured Caco-2 cell upon K8 loss, but it could be due to compensatory expression in Caco-2 colon cancer cells. As $\Delta\Psi m$ is the main driver of mitochondrial Ca^{2+} entry (61), the decreased $\Delta\Psi m$ in K8$^{-/-}$ Caco-2 cells may partly underlie the reduced Ca^{2+} uptake. Another possibility is that K8 loss impacts mitochondrial interactions with other organelles. As MCU has a low affinity for Ca^{2+}, mitochondrial Ca^{2+} uptake occurs close to the plasma membrane, endoplasmic reticulum (ER), or sarcoplasmic reticulum (SR), where Ca^{2+} levels are higher (41, 62, 63). Mitochondria and the ER are linked by protein tethers at specific ER membrane sites termed mitochondria-associated membranes (64, 65), where complexes of ER inositol 1,4,5-trisphosphate receptors (IP_3Rs), grp75, and VDAC facilitate ER-mitochondria Ca^{2+} flux (66). As IP_3Rs are essential for ER-mitochondria linkage (67), mitochondria-ER tethering may be reduced in K8$^{-/-}$ mouse colonocytes due to the downregulation of VDAC. This is supported by studies showing that desmin may bind VDAC (68) and that aggregate-prone desmin mutations are associated with decreased mitochondrial Ca^{2+} uptake, likely due to loss of mitochondria-SR interactions (63). Interestingly, plectin 1b has been speculated to bind VDAC (48), raising the possibility that K8 or another partner keratin could bind VDAC directly or indirectly through, for example, plectin. Mitofusin-2 has also been implicated as a mitochondria-ER tether, as mitofusin-2 deficiency increases the distance between mitochondria and the ER and reduces mitochondrial Ca^{2+} uptake (44, 69). However, several reports either support or challenge this notion, and the matter remains subject to further study (44, 69–75). As mitofusin-2 is involved in the regulation of mitochondrial dynamics and

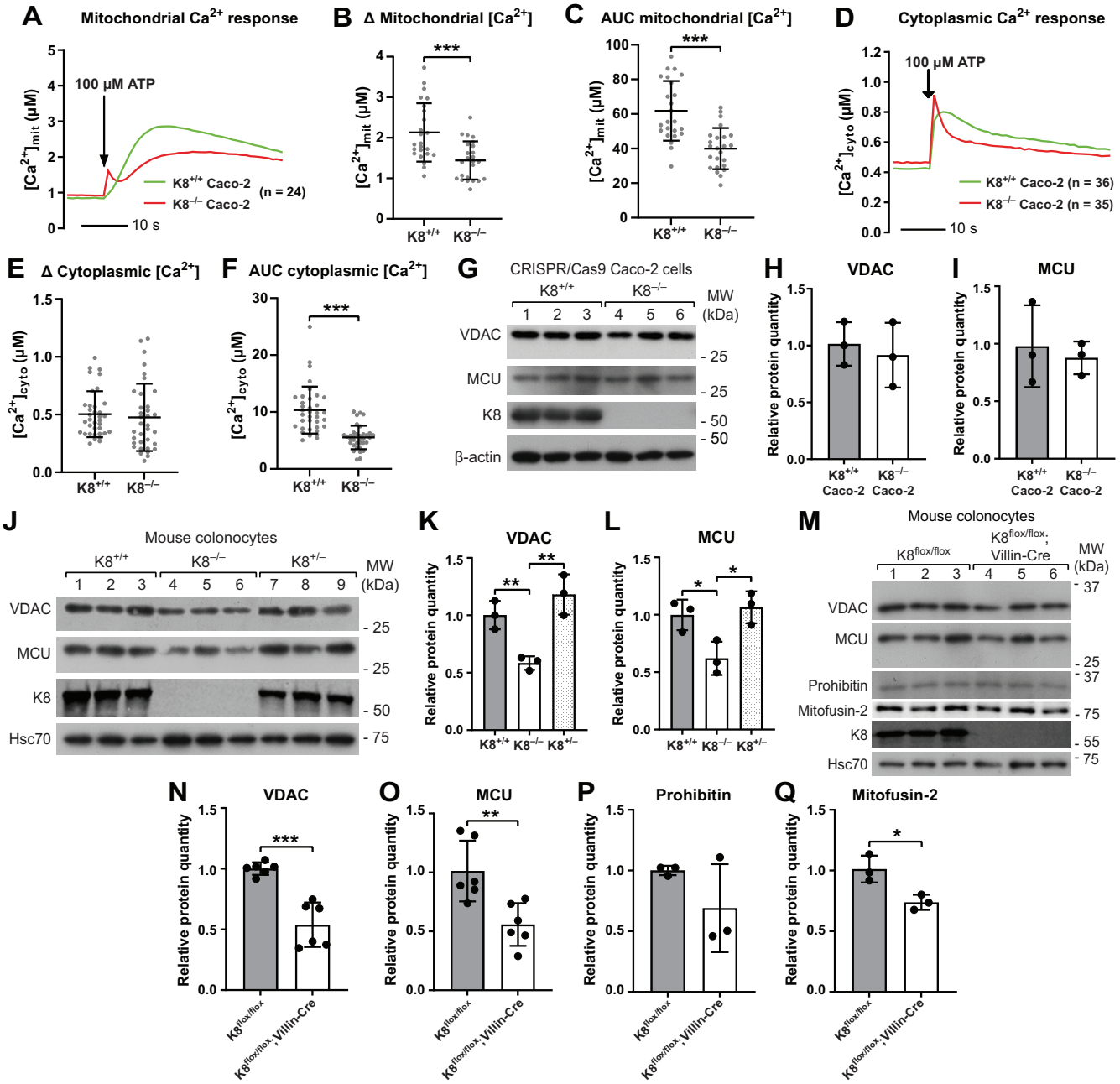

Figure 7. The mitochondrial Ca^{2+} response is attenuated in Caco-2 $K8^{-/-}$ cells and colonic epithelium of mice lacking K8. *A* and *D*: $K8^{+/+}$ and $K8^{-/-}$ Caco-2 cells were transfected with aequorin targeted to the mitochondrial matrix (mito-Aeq; *A*) or untagged aequorin (*D*; no target, cytoplasmic localization), and Ca^{2+} responses were measured following stimulation with ATP. Representative mitochondrial (*A*) and cytoplasmic (*D*) Ca^{2+} responses are shown. *B*, *C*, *E*, and *F*: changes in mitochondrial and cytoplasmic Ca^{2+} levels were quantified and displayed as Δ (maximum – minimum) Ca^{2+} concentration ($[Ca^{2+}]$) (*B* and *E*) and area under the curve (AUC) $[Ca^{2+}]$ (*C* and *F*). The results represent the average Ca^{2+} responses ($n = 24$/genotype for mitochondrial $[Ca^{2+}]$ and $n = 35$–36/genotype for cytoplasmic $[Ca^{2+}]$ from 3 experiments; small dots represent individual values) ± SD with significant differences shown: ***$P < 0.001$. *G–L*: $K8^{+/+}$ and $K8^{-/-}$ Caco-2 cells (*G–I*) and isolated colonocytes from male $K8^{+/+}$, $K8^{-/-}$, and $K8^{+/-}$ mice (*J–L*) were analyzed by immunoblotting for the mitochondrial Ca^{2+} transporters voltage-dependent anion channel (VDAC) and mitochondrial calcium uniporter (MCU). The K8 genotype is shown by the K8 blots (notably, the same K8 blot is shown in Figs. 5*A* and 7*G*, as both used the same Caco-2 sample set, and, similarly, the same K8 blot is shown in Figs. 6*A* and 7*J*, as both used the same mouse colonocyte sample set). The immunoblots were quantified and normalized against β-actin or Hsc70. The results represent the average ($n = 3$/genotype) fold change relative to $K8^{+/+}$ ± SD, with significant differences shown: *$P < 0.05$ and **$P < 0.01$. *M–Q*: VDAC, MCU, prohibitin, and mitofusin-2 protein levels were determined in male and female $K8^{flox/flox}$ and $K8^{flox/flox}$;Villin-Cre (endogenous K8 knockdown) mouse colonocytes by immunoblotting (a representative Western blot is shown). The immunoblots were quantified and normalized against Hsc70. The results represent the average fold change relative to $K8^{+/+}$ ± SD ($n = 6$ mice/genotype for VDAC and MCU; $n = 3$ mice/genotype for prohibitin and mitofusin-2) with significant differences shown: *$P < 0.05$, **$P < 0.01$, and ***$P < 0.001$. MW (kDa) indicates the closest molecular mass marker on the Western blots.

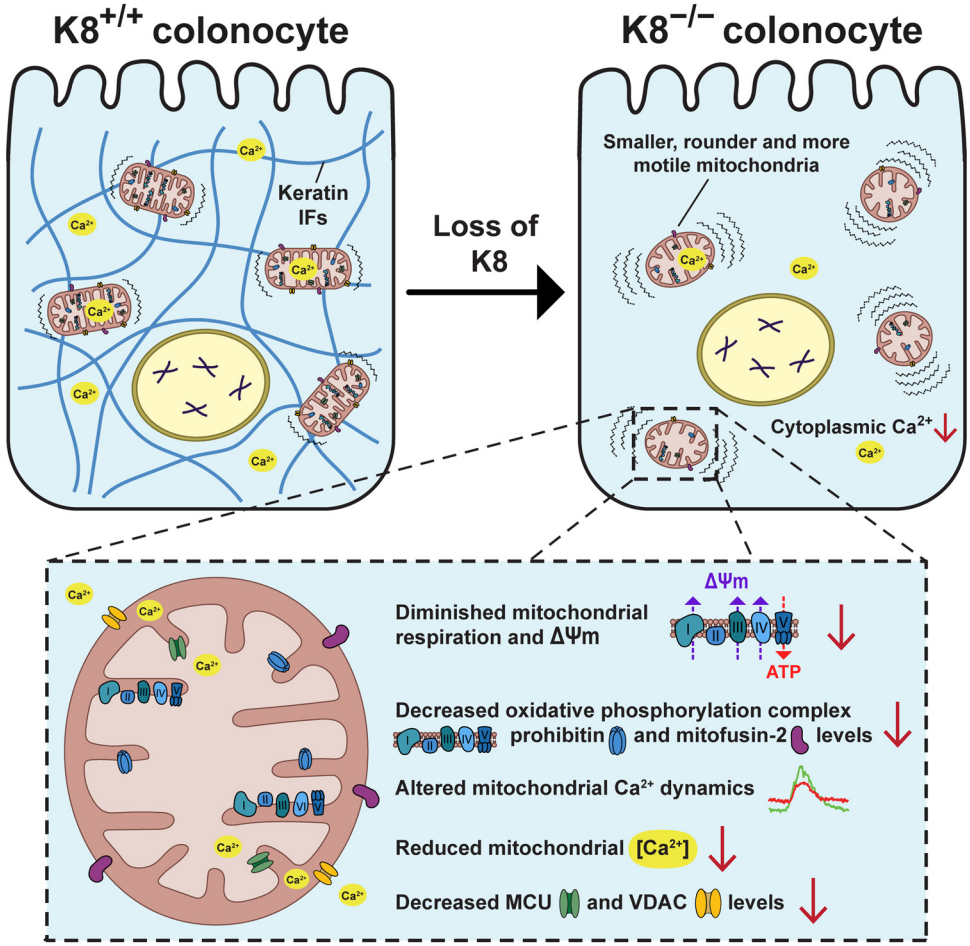

Figure 8. Graphical summary. K8 stabilizes mitochondria by restricting mitochondrial movement and contributes to maintaining mitochondrial size, shape, energy metabolism, and Ca^{2+} signaling in colonocytes. In the absence of K8, colonocyte mitochondria are smaller, rounder, and more motile. $K8^{-/-}$ mitochondria also display diminished respiration and mitochondrial membrane potential ($\Delta\Psi m$) and decreased oxidative phosphorylation complex, prohibitin, and mitofusin-2 protein levels. Furthermore, Ca^{2+} levels are decreased and Ca^{2+} dynamics are altered in the mitochondrial matrix and cytoplasm of $K8^{-/-}$ Caco-2 cells, while the mitochondrial Ca^{2+} transporters voltage-dependent anion channel (VDAC) and mitochondrial calcium uniporter (MCU) are downregulated in $K8^{-/-}$ mouse colonocytes. Taken together, the above-mentioned alterations in mitochondrial dynamics and function are likely contributing factors to the diminished mitochondrial energy metabolism in $K8^{-/-}$ colonocytes and may contribute to K8-associated colitis pathophysiology. [Ca^{2+}], Ca^{2+} concentration; IFs, intermediate filaments.

mitochondria-ER cross talk, the reduced mitofusin-2 protein levels in $K8^{-/-}$ Caco-2 cells, which can be rescued by reexpression of K8/K18, could potentially explain why mitochondrial Ca^{2+} uptake is perturbed in these cells. Finally, while the cytoplasmic Ca^{2+} changes can in part reflect the changes in mitochondrial matrix Ca^{2+}, these data suggest that K8-mediated processes may also play a role in cytoplasmic Ca^{2+} signaling. All in all, these results, together with findings that desmin regulates Ca^{2+} signaling (63, 76), support an important role for keratins and IFs in Ca^{2+} homeostasis.

While IFs have many cell- and tissue-specific functions, this study clearly adds to the growing number of evidence showing a common IF function in mitochondrial regulation independent of IF type, cell type or type of energy source. A clear molecular mechanism for how IFs, and keratins in particular, interact with and regulate mitochondria, however, remains elusive. Some IFs, including vimentin and desmin, can directly bind to and regulate mitochondria (45, 48, 77). Intriguingly, K18 contains an NH_2-terminal amino acid sequence, which could potentially facilitate direct interaction between keratin IFs and the OMM (48). IF-mitochondria interactions can also occur indirectly through IF-associated proteins. In regard to keratins, the linker protein trichoplein (43, 78), which can bind both keratins and mitofusin-2, has been suggested to facilitate keratin-mitochondria interactions in β-cells, as both trichoplein and mitofusin-2 are downregulated upon K8 loss (7). Similarly, mitofusin-2 protein levels are significantly decreased both in vitro and in vivo in colonocytes upon K8 loss; however, trichoplein protein levels were unaltered. These observations suggest that the mitochondrial shape changes in $K8^{-/-}$ colonocytes may at least partly be caused by the mitofusin-2 deficiency (53), while changes in trichoplein protein levels likely are dispensable for this phenotype. However, directed mitochondrial movement increases considerably upon trichoplein loss (79), indicating that keratin-trichoplein interactions may be instrumental in keratin-mediated regulation of mitochondrial movement. The cytolinker protein plectin, which links vimentin and desmin to mitochondria (45, 80–82), is another potential candidate for anchoring K8 to mitochondria. Indeed, it has been reported that plectin mediates K8-mitochondria interactions in the retinal pigment epithelium and that K8 phosphorylation disrupts this interaction (83). We have recently shown that plectin is downregulated in $K8^{-/-}$ colonocytes, indicating that the coupling of keratins and nuclei is lost (6). It is thus plausible that plectin could mediate the association between keratins and mitochondria in colonocytes. In addition, mitochondrial trichoplein levels are reduced upon plectin 1b silencing in HeLa cells (43), indicating that plectin may play a role in facilitating keratin-trichoplein interactions at mitochondria. Based on these observations by us and others, we propose that K8 tethers and stabilizes mitochondria in colonocytes, thus maintaining mitochondrial shape and size. However, further research is warranted to elucidate the exact molecular mechanism for keratin-mitochondria interactions.

Based on the finding that butyrate oxidation is decreased in the colonic mucosa in ulcerative colitis, Roediger (84) proposed that ulcerative colitis could be characterized as an energy-deficiency disease. Veritably, mitochondrial dysfunction is increasingly recognized as a contributing factor to IBD pathogenesis (85). For instance, ulcerative colitis has been characterized by downregulation of both respiratory chain complex levels and activity and reduced $\Delta\Psi m$ (86, 87). Similarly, Crohn's disease has been associated with dysfunctional mitochondrial metabolism (88, 89). Further, Crohn's disease in pediatric patients is characterized by a depletion of butyrate-producing bacteria, the levels of which appeared to correlate with mitochondrial protein levels, suggesting a role for butyrate in mitochondrial regulation (89). As $K8^{-/-}$ colon epithelium displays several of the hallmarks of dysfunctional energy metabolism in IBD, including reduced butyrate uptake (22, 90) and diminished mitochondrial respiration, we propose that the changes in mitochondrial dynamics and metabolism presented here may contribute to K8-associated colitis pathophysiology.

DATA AVAILABILITY

The authors confirm that the data supporting the findings of this study are available within the article. Data will be made available upon reasonable request.

ACKNOWLEDGMENTS

We are very grateful to Karen Ridge (Northwestern University Feinberg School of Medicine) for the $K8^{flox/flox}$ mouse strain and thank Carl-Gustav Stenvall (Åbo Akademi University) for breeding and providing $K8^{flox/flox}$ and $K8^{flox/flox}$;Villin-Cre mice. We are grateful to members of the Toivola Epithelial Biology laboratory (Åbo Akademi University) for assistance and comments. Imaging/Flow cytometry was performed at the Cell Imaging and Cytometry Core, Turku Bioscience Centre, Turku, Finland, with the support of Biocenter Finland.

GRANTS

This work was supported by the Research Council of Finland (140759, 126161, 332582, and 315139; to D.M.T.), EU FP7 IRG (to D.M.T.), European Cooperation in Science and Technology (COST) Action CA15214 (EuroCellNet; to D.M.T.), the InFLAMES Flagship Program of the Academy of Finland (337531 and 357911; to D.M.T.), K. Albin Johansson Foundation (to J.H.N.), Otto A. Malm Foundation (to J.H.N.), Magnus Ehrnrooth Foundation (to J.H.N.), Makarna Agneta och Carl-Erik Olins Foundation (to J.H.N.), Mary and Georg C. Ehrnrooths Foundation (to T.R.H.H.), Medicinska Understödsföreningen Liv och Hälsa (to D.M.T. and J.H.N.), the Paulo Foundation (to T.R.H.H.), Sigrid Jusélius Stiftelse (to D.M.T.), Svenska Kulturfonden (to J.H.N.), Turku Doctoral Program in Molecular Biosciences at Åbo Akademi University (to J.H.N.), Victoriastiftelsen (to J.H.N.), Waldemar von Frenckells Foundation (to J.H.N.), Åbo Akademi University Centers of Excellence of Cell Stress and Molecular Aging and Cellular Mechanostasis (to D.M.T.), and Åbo Akademi University (to J.H.N. and T.R.H.H.).

DISCLOSURES

No conflicts of interest, financial or otherwise, are declared by the authors.

AUTHOR CONTRIBUTIONS

J.H.N., T.R.H.H., K.T., I.P., K.T., and D.M.T. conceived and designed research; J.H.N., T.R.H.H., K.T., and I.P. performed experiments; J.H.N., T.R.H.H., K.T., I.P., K.T., and D.M.T. analyzed data; J.H.N., T.R.H.H., K.T., I.P., K.T., and D.M.T. interpreted results of experiments; J.H.N. and T.R.H.H. prepared figures; J.H.N. and T.R.H.H. drafted manuscript; J.H.N., T.R.H.H., K.T., I.P., K.T., and D.M.T. edited and revised manuscript; J.H.N., T.R.H.H., K.T., I.P., K.T., and D.M.T. approved final version of manuscript.

REFERENCES

1. **Schweizer J**, **Bowden PE**, **Coulombe PA**, **Langbein L**, **Lane EB**, **Magin TM**, **Maltais L**, **Omary MB**, **Parry DA**, **Rogers MA**, **Wright MW.** New consensus nomenclature for mammalian keratins. *J Cell Biol* 174: 169–174, 2006. doi:10.1083/jcb.200603161.
2. **Coulombe PA**, **Omary MB.** 'Hard' and 'soft' principles defining the structure, function and regulation of keratin intermediate filaments. *Curr Opin Cell Biol* 14: 110–122, 2002. doi:10.1016/s0955-0674(01)00301-5.
3. **Polari L**, **Alam CM**, **Nyström JH**, **Heikkilä T**, **Tayyab M**, **Baghestani S**, **Toivola DM.** Keratin intermediate filaments in the colon: guardians of epithelial homeostasis. *Int J Biochem Cell Biol* 129: 105878, 2020. doi:10.1016/j.biocel.2020.105878.
4. **Toivola DM**, **Tao GZ**, **Habtezion A**, **Liao J**, **Omary MB.** Cellular integrity plus: organelle-related and protein-targeting functions of intermediate filaments. *Trends Cell Biol* 15: 608–617, 2005. doi:10.1016/j.tcb.2005.09.004.
5. **Omary MB.** Intermediate filament proteins of digestive organs: physiology and pathophysiology. *Am J Physiol Gastrointest Liver Physiol* 312: G628–G634, 2017. doi:10.1152/ajpgi.00455.2016.
6. **Stenvall CA**, **Nyström JH**, **Butler-Hallissey C**, **Jansson T**, **Heikkilä T**, **Adam SA**, **Foisner R**, **Goldman RD**, **Ridge KM**, **Toivola DM.** Cytoplasmic keratins couple with and maintain nuclear envelope integrity in colonic epithelial cells. *Mol Biol Cell* 33: ar121, 2022. mbcE20060387. doi:10.1091/mbc.E20-06-0387.
7. **Silvander JSG**, **Kvarnström SM**, **Kumari-Ilieva A**, **Shrestha A**, **Alam CM**, **Toivola DM.** Keratins regulate beta-cell mitochondrial morphology, motility, and homeostasis. *FASEB J* 31: 4578–4587, 2017. doi:10.1096/fj.201700095R.
8. **Steen K**, **Chen D**, **Wang F**, **Majumdar R**, **Chen S**, **Kumar S**, **Lombard DB**, **Weigert R**, **Zieman AG**, **Parent CA**, **Coulombe PA.** A role for keratins in supporting mitochondrial organization and function in skin keratinocytes. *Mol Biol Cell* 31: 1103–1111, 2020. doi:10.1091/mbc.E19-10-0565.
9. **Lee CH**, **Kim MS**, **Chung BM**, **Leahy DJ**, **Coulombe PA.** Structural basis for heteromeric assembly and perinuclear organization of keratin filaments. *Nat Struct Mol Biol* 19: 707–715, 2012. doi:10.1038/nsmb.2330.
10. **Toivola DM**, **Boor P**, **Alam C**, **Strnad P.** Keratins in health and disease. *Curr Opin Cell Biol* 32: 73–81, 2015. doi:10.1016/j.ceb.2014.12.008.
11. **Coulombe PA**, **Hutton ME**, **Letai A**, **Hebert A**, **Paller AS**, **Fuchs E.** Point mutations in human keratin 14 genes of epidermolysis bullosa simplex patients: genetic and functional analyses. *Cell* 66: 1301–1311, 1991. doi:10.1016/0092-8674(91)90051-y.
12. **Ku NO**, **Darling JM**, **Krams SM**, **Esquivel CO**, **Keeffe EB**, **Sibley RK**, **Lee YM**, **Wright TL**, **Omary MB.** Keratin 8 and 18 mutations are risk factors for developing liver disease of multiple etiologies. *Proc Natl Acad Sci USA* 100: 6063–6068, 2003. doi:10.1073/pnas.0936165100.
13. **Owens DW**, **Wilson NJ**, **Hill AJ**, **Rugg EL**, **Porter RM**, **Hutcheson AM**, **Quinlan RA**, **van Heel D**, **Parkes M**, **Jewell DP**, **Campbell SS**, **Ghosh S**, **Satsangi J**, **Lane EB.** Human keratin 8 mutations that disturb filament assembly observed in inflammatory bowel disease patients. *J Cell Sci* 117: 1989–1999, 2004. doi:10.1242/jcs.01043.
14. **Polari L**, **Tenhami M**, **Anttila S**, **Helenius T**, **Kujari H**, **Kallajoki M**, **Voutilainen M**, **Toivola DM.** Colonocyte keratin 7 is expressed de novo in inflammatory bowel diseases and associated with pathological changes and drug-resistance. *Sci Rep* 12: 22213, 2022. doi:10.1038/s41598-022-26603-2.
15. **Stenvall CA**, **Tayyab M**, **Grönroos TJ**, **Ilomäki MA**, **Viiri K**, **Ridge KM**, **Polari L**, **Toivola DM.** Targeted deletion of keratin 8 in intestinal epithelial cells disrupts tissue integrity and predisposes to

tumorigenesis in the colon. *Cell Mol Life Sci* 79: 10, 2021. doi:10.1007/s00018-021-04081-5.
16. **Baribault H**, **Penner J**, **Iozzo RV**, **Wilson-Heiner M.** Colorectal hyperplasia and inflammation in keratin 8-deficient FVB/N mice. *Genes Dev* 8: 2964–2973, 1994. doi:10.1101/gad.8.24.2964.
17. **Asghar MN**, **Priyamvada S**, **Nyström JH**, **Anbazhagan AN**, **Dudeja PK**, **Toivola DM.** Keratin 8 knockdown leads to loss of the chloride transporter DRA in the colon. *Am J Physiol Gastrointest Liver Physiol* 310: G1147–G1154, 2016. doi:10.1152/ajpgi.00354.2015.
18. **Misiorek JO**, **Lähdeniemi IAK**, **Nyström JH**, **Paramonov VM**, **Gullmets JA**, **Saarento H**, **Rivero-Muller A**, **Husøy T**, **Taimen P**, **Toivola DM.** Keratin 8-deletion induced colitis predisposes to murine colorectal cancer enforced by the inflammasome and IL-22 pathway. *Carcinogenesis* 37: 777–786, 2016. doi:10.1093/carcin/bgw063.
19. **Toivola DM**, **Krishnan S**, **Binder HJ**, **Singh SK**, **Omary MB.** Keratins modulate colonocyte electrolyte transport via protein mistargeting. *J Cell Biol* 164: 911–921, 2004. doi:10.1083/jcb.200308103.
20. **Lähdeniemi IAK**, **Misiorek JO**, **Antila CJM**, **Landor SK**, **Stenvall CA**, **Fortelius LE**, **Bergstrom LK**, **Sahlgren C**, **Toivola DM.** Keratins regulate colonic epithelial cell differentiation through the Notch1 signalling pathway. *Cell Death Differ* 24: 984–996, 2017. doi:10.1038/cdd.2017.28.
21. **Asghar MN**, **Silvander JS**, **Helenius TO**, **Lahdeniemi IA**, **Alam C**, **Fortelius LE**, **Holmsten RO**, **Toivola DM.** The amount of keratins matters for stress protection of the colonic epithelium. *PLoS One* 10: e0127436, 2015. doi:10.1371/journal.pone.0127436.
22. **Helenius TO**, **Misiorek JO**, **Nyström JH**, **Fortelius LE**, **Habtezion A**, **Liao J**, **Asghar MN**, **Zhang H**, **Azhar S**, **Omary MB**, **Toivola DM.** Keratin 8 absence down-regulates colonocyte HMGCS2 and modulates colonic ketogenesis and energy metabolism. *Mol Biol Cell* 26: 2298–2310, 2015. doi:10.1091/mbc.E14-02-0736.
23. **Rizzuto R**, **De Stefani D**, **Raffaello A**, **Mammucari C.** Mitochondria as sensors and regulators of calcium signalling. *Nat Rev Mol Cell Biol* 13: 566–578, 2012. doi:10.1038/nrm3412.
24. **Kasahara A**, **Scorrano L.** Mitochondria: from cell death executioners to regulators of cell differentiation. *Trends Cell Biol* 24: 761–770, 2014. doi:10.1016/j.tcb.2014.08.005.
25. **Giacomello M**, **Pyakurel A**, **Glytsou C**, **Scorrano L.** The cell biology of mitochondrial membrane dynamics. *Nat Rev Mol Cell Biol* 21: 204–224, 2020. doi:10.1038/s41580-020-0210-7.
26. **Schwarz N**, **Leube RE.** Intermediate filaments as organizers of cellular space: how they affect mitochondrial structure and function. *Cells* 5: 30, 2016. doi:10.3390/cells5030030.
27. **Shah M**, **Chacko LA**, **Joseph JP**, **Ananthanarayanan V.** Mitochondrial dynamics, positioning and function mediated by cytoskeletal interactions. *Cell Mol Life Sci* 78: 3969–3986, 2021. doi:10.1007/s00018-021-03762-5.
28. **Tao GZ**, **Looi KS**, **Toivola DM**, **Strnad P**, **Zhou Q**, **Liao J**, **Wei Y**, **Habtezion A**, **Omary MB.** Keratins modulate the shape and function of hepatocyte mitochondria: a mechanism for protection from apoptosis. *J Cell Sci* 122: 3851–3855, 2009. doi:10.1242/jcs.051862.
29. **Lehmann SM**, **Leube RE**, **Schwarz N.** Keratin 6a mutations lead to impaired mitochondrial quality control. *Br J Dermatol* 182: 636–647, 2020. doi:10.1111/bjd.18014.
30. **Kumar V**, **Bouameur JE**, **Bar J**, **Rice RH**, **Hornig-Do HT**, **Roop DR**, **Schwarz N**, **Brodesser S**, **Thiering S**, **Leube RE**, **Wiesner RJ**, **Vijayaraj P**, **Brazel CB**, **Heller S**, **Binder H**, **Loffler-Wirth H**, **Seibel P**, **Magin TM.** A keratin scaffold regulates epidermal barrier formation, mitochondrial lipid composition, and activity. *J Cell Biol* 211: 1057–1075, 2015 [Erratum in J Cell Biol 212: 877, 2016]. doi:10.1083/jcb.201404147.
31. **Vetter A**, **Jahn K**, **Bouameur JE**, **Kiritsi D**, **Magin TM.** Epidermolysis bullosa simplex keratinocytes show disturbed mitochondrial positioning and activity. *J Invest Dermatol* 140: 1438–1442 e1435, 2020. doi:10.1016/j.jid.2019.10.023.
32. **Alvarado DM**, **Coulombe PA.** Directed expression of a chimeric type II keratin partially rescues keratin 5-null mice. *J Biol Chem* 289: 19435–19447, 2014. doi:10.1074/jbc.M114.553867.
33. **Donohoe DR**, **Garge N**, **Zhang X**, **Sun W**, **O'Connell TM**, **Bunger MK**, **Bultman SJ.** The microbiome and butyrate regulate energy metabolism and autophagy in the mammalian colon. *Cell Metab* 13: 517–526, 2011. doi:10.1016/j.cmet.2011.02.018.
34. **Roediger WE.** Role of anaerobic bacteria in the metabolic welfare of the colonic mucosa in man. *Gut* 21: 793–798, 1980. doi:10.1136/gut.21.9.793.
35. **Bonora M**, **Giorgi C**, **Bononi A**, **Marchi S**, **Patergnani S**, **Rimessi A**, **Rizzuto R**, **Pinton P.** Subcellular calcium measurements in mammalian cells using jellyfish photoprotein aequorin-based probes. *Nat Protoc* 8: 2105–2118, 2013. doi:10.1038/nprot.2013.127.
36. **Schindelin J**, **Arganda-Carreras I**, **Frise E**, **Kaynig V**, **Longair M**, **Pietzsch T**, **Preibisch S**, **Rueden C**, **Saalfeld S**, **Schmid B**, **Tinevez JY**, **White DJ**, **Hartenstein V**, **Eliceiri K**, **Tomancak P**, **Cardona A.** Fiji: an open-source platform for biological-image analysis. *Nat Methods* 9: 676–682, 2012. doi:10.1038/nmeth.2019.
37. **Signorile A**, **Sgaramella G**, **Bellomo F**, **De Rasmo D.** Prohibitins: a critical role in mitochondrial functions and implication in diseases. *Cells* 8: 71, 2019. doi:10.3390/cells8010071.
38. **Mourier A**, **Motori E**, **Brandt T**, **Lagouge M**, **Atanassov I**, **Galinier A**, **Rappl G**, **Brodesser S**, **Hultenby K**, **Dieterich C**, **Larsson NG.** Mitofusin 2 is required to maintain mitochondrial coenzyme Q levels. *J Cell Biol* 208: 429–442, 2015. doi:10.1083/jcb.201411100.
39. **Sebastian D**, **Hernandez-Alvarez MI**, **Segales J**, **Sorianello E**, **Munoz JP**, **Sala D**, **Waget A**, **Liesa M**, **Paz JC**, **Gopalacharyulu P**, **Oresic M**, **Pich S**, **Burcelin R**, **Palacin M**, **Zorzano A.** Mitofusin 2 (Mfn2) links mitochondrial and endoplasmic reticulum function with insulin signaling and is essential for normal glucose homeostasis. *Proc Natl Acad Sci USA* 109: 5523–5528, 2012. doi:10.1073/pnas.1108220109.
40. **Pich S**, **Bach D**, **Briones P**, **Liesa M**, **Camps M**, **Testar X**, **Palacin M**, **Zorzano A.** The Charcot-Marie-Tooth type 2A gene product, Mfn2, up-regulates fuel oxidation through expression of OXPHOS system. *Hum Mol Genet* 14: 1405–1415, 2005. doi:10.1093/hmg/ddi149.
41. **Rossi A**, **Pizzo P**, **Filadi R.** Calcium, mitochondria and cell metabolism: a functional triangle in bioenergetics. *Biochim Biophys Acta Mol Cell Res* 1866: 1068–1078, 2019. doi:10.1016/j.bbamcr.2018.10.016.
42. **Modesti L**, **Danese A**, **Angela Maria Vitto V**, **Ramaccini D**, **Aguiari G**, **Gafa R**, **Lanza G**, **Giorgi C**, **Pinton P.** Mitochondrial Ca^{2+} signaling in health, disease, and therapy. *Cells* 10: 1317, 2021. doi:10.3390/cells10061317.
43. **Cerqua C**, **Anesti V**, **Pyakurel A**, **Liu D**, **Naon D**, **Wiche G**, **Baffa R**, **Dimmer KS**, **Scorrano L.** Trichoplein/mitostatin regulates endoplasmic reticulum-mitochondria juxtaposition. *EMBO Rep* 11: 854–860, 2010. doi:10.1038/embor.2010.151.
44. **de Brito OM**, **Scorrano L.** Mitofusin 2 tethers endoplasmic reticulum to mitochondria. *Nature* 456: 605–610, 2008 [Erratum in Nature 513: 266, 2014]. doi:10.1038/nature07534.
45. **Nekrasova OE**, **Mendez MG**, **Chernoivanenko IS**, **Tyurin-Kuzmin PA**, **Kuczmarski ER**, **Gelfand VI**, **Goldman RD**, **Minin AA.** Vimentin intermediate filaments modulate the motility of mitochondria. *Mol Biol Cell* 22: 2282–2289, 2011. doi:10.1091/mbc.E10-09-0766.
46. **Gentil BJ**, **Minotti S**, **Beange M**, **Baloh RH**, **Julien JP**, **Durham HD.** Normal role of the low-molecular-weight neurofilament protein in mitochondrial dynamics and disruption in Charcot-Marie-Tooth disease. *FASEB J* 26: 1194–1203, 2012. doi:10.1096/fj.11-196345.
47. **Milner DJ**, **Mavroidis M**, **Weisleder N**, **Capetanaki Y.** Desmin cytoskeleton linked to muscle mitochondrial distribution and respiratory function. *J Cell Biol* 150: 1283–1298, 2000. doi:10.1083/jcb.150.6.1283.
48. **Chernoivanenko IS**, **Matveeva EA**, **Gelfand VI**, **Goldman RD**, **Minin AA.** Mitochondrial membrane potential is regulated by vimentin intermediate filaments. *FASEB J* 29: 820–827, 2015. doi:10.1096/fj.14-259903.
49. **Matveeva EA**, **Venkova LS**, **Chernoivanenko IS**, **Minin AA.** Vimentin is involved in regulation of mitochondrial motility and membrane potential by Rac1. *Biol Open* 4: 1290–1297, 2015. doi:10.1242/bio.011874.
50. **Winter L**, **Kuznetsov AV**, **Grimm M**, **Zeold A**, **Fischer I**, **Wiche G.** Plectin isoform P1b and P1d deficiencies differentially affect mitochondrial morphology and function in skeletal muscle. *Hum Mol Genet* 24: 4530–4544, 2015. doi:10.1093/hmg/ddv184.
51. **Cogliati S**, **Frezza C**, **Soriano ME**, **Varanita T**, **Quintana-Cabrera R**, **Corrado M**, **Cipolat S**, **Costa V**, **Casarin A**, **Gomes LC**, **Perales-Clemente E**, **Salviati L**, **Fernandez-Silva P**, **Enriquez JA**, **Scorrano L.** Mitochondrial cristae shape determines respiratory chain supercomplexes assembly and respiratory efficiency. *Cell* 155: 160–171, 2013. doi:10.1016/j.cell.2013.08.032.

52. **Nielsen J**, **Gejl KD**, **Hey-Mogensen M**, **Holmberg HC**, **Suetta C**, **Krustrup P**, **Elemans CPH**, **Ortenblad N.** Plasticity in mitochondrial cristae density allows metabolic capacity modulation in human skeletal muscle. *J Physiol* 595: 2839–2847, 2017. doi:10.1113/JP273040.
53. **Chen H**, **Chomyn A**, **Chan DC.** Disruption of fusion results in mitochondrial heterogeneity and dysfunction. *J Biol Chem* 280: 26185–26192, 2005. doi:10.1074/jbc.M503062200.
54. **Rossignol R**, **Gilkerson R**, **Aggeler R**, **Yamagata K**, **Remington SJ**, **Capaldi RA.** Energy substrate modulates mitochondrial structure and oxidative capacity in cancer cells. *Cancer Res* 64: 985–993, 2004. doi:10.1158/0008-5472.can-03-1101.
55. **Overly CC**, **Rieff HI**, **Hollenbeck PJ.** Organelle motility and metabolism in axons vs dendrites of cultured hippocampal neurons. *J Cell Sci* 109: 971–980, 1996. doi:10.1242/jcs.109.5.971.
56. **Segales J**, **Paz JC**, **Hernandez-Alvarez MI**, **Sala D**, **Munoz JP**, **Noguera E**, **Pich S**, **Palacin M**, **Enriquez JA**, **Zorzano A.** A form of mitofusin 2 (Mfn2) lacking the transmembrane domains and the COOH-terminal end stimulates metabolism in muscle and liver cells. *Am J Physiol Endocrinol Metab* 305: E1208–E1221, 2013 [Erratum in Am J Physiol Endocrinol Metab 306: E580, 2014]. doi:10.1152/ajpendo.00546.2012.
57. **Bach D**, **Pich S**, **Soriano FX**, **Vega N**, **Baumgartner B**, **Oriola J**, **Daugaard JR**, **Lloberas J**, **Camps M**, **Zierath JR**, **Rabasa-Lhoret R**, **Wallberg-Henriksson H**, **Laville M**, **Palacin M**, **Vidal H**, **Rivera F**, **Brand M**, **Zorzano A.** Mitofusin-2 determines mitochondrial network architecture and mitochondrial metabolism. A novel regulatory mechanism altered in obesity. *J Biol Chem* 278: 17190–17197, 2003. doi:10.1074/jbc.M212754200.
58. **Nijtmans LG**, **de Jong L**, **Artal Sanz M**, **Coates PJ**, **Berden JA**, **Back JW**, **Muijsers AO**, **van der Spek H**, **Grivell LA.** Prohibitins act as a membrane-bound chaperone for the stabilization of mitochondrial proteins. *EMBO J* 19: 2444–2451, 2000. doi:10.1093/emboj/19.11.2444.
59. **Bourges I**, **Ramus C**, **Mousson de Camaret B**, **Beugnot R**, **Remacle C**, **Cardol P**, **Hofhaus G**, **Issartel JP.** Structural organization of mitochondrial human complex I: role of the ND4 and ND5 mitochondria-encoded subunits and interaction with prohibitin. *Biochem J* 383: 491–499, 2004. doi:10.1042/BJ20040256.
60. **Tsutsumi T**, **Matsuda M**, **Aizaki H**, **Moriya K**, **Miyoshi H**, **Fujie H**, **Shintani Y**, **Yotsuyanagi H**, **Miyamura T**, **Suzuki T**, **Koike K.** Proteomics analysis of mitochondrial proteins reveals overexpression of a mitochondrial protein chaperon, prohibitin, in cells expressing hepatitis C virus core protein. *Hepatology* 50: 378–386, 2009. doi:10.1002/hep.22998.
61. **Kirichok Y**, **Krapivinsky G**, **Clapham DE.** The mitochondrial calcium uniporter is a highly selective ion channel. *Nature* 427: 360–364, 2004. doi:10.1038/nature02246.
62. **Rizzuto R**, **Pinton P**, **Carrington W**, **Fay FS**, **Fogarty KE**, **Lifshitz LM**, **Tuft RA**, **Pozzan T.** Close contacts with the endoplasmic reticulum as determinants of mitochondrial Ca^{2+} responses. *Science* 280: 1763–1766, 1998. doi:10.1126/science.280.5370.1763.
63. **Smolina N**, **Bruton J**, **Sjoberg G**, **Kostareva A**, **Sejersen T.** Aggregate-prone desmin mutations impair mitochondrial calcium uptake in primary myotubes. *Cell Calcium* 56: 269–275, 2014. doi:10.1016/j.ceca.2014.08.001.
64. **Vance JE.** MAM (mitochondria-associated membranes) in mammalian cells: lipids and beyond. *Biochim Biophys Acta* 1841: 595–609, 2014. doi:10.1016/j.bbalip.2013.11.014.
65. **Csordas G**, **Renken C**, **Varnai P**, **Walter L**, **Weaver D**, **Buttle KF**, **Balla T**, **Mannella CA**, **Hajnoczky G.** Structural and functional features and significance of the physical linkage between ER and mitochondria. *J Cell Biol* 174: 915–921, 2006. doi:10.1083/jcb.200604016.
66. **Szabadkai G**, **Bianchi K**, **Varnai P**, **De Stefani D**, **Wieckowski MR**, **Cavagna D**, **Nagy AI**, **Balla T**, **Rizzuto R.** Chaperone-mediated coupling of endoplasmic reticulum and mitochondrial Ca^{2+} channels. *J Cell Biol* 175: 901–911, 2006. doi:10.1083/jcb.200608073.
67. **Bartok A**, **Weaver D**, **Golenar T**, **Nichtova Z**, **Katona M**, **Bansaghi S**, **Alzayady KJ**, **Thomas VK**, **Ando H**, **Mikoshiba K**, **Joseph SK**, **Yule DI**, **Csordas G**, **Hajnoczky G.** IP(3) receptor isoforms differently regulate ER-mitochondrial contacts and local calcium transfer. *Nat Commun* 10: 3726, 2019. doi:10.1038/s41467-019-11646-3.
68. **Diokmetzidou A**, **Soumaka E**, **Kloukina I**, **Tsikitis M**, **Makridakis M**, **Varela A**, **Davos CH**, **Georgopoulos S**, **Anesti V**, **Vlahou A**, **Capetanaki Y.** Desmin and alphaB-crystallin interplay in the maintenance of mitochondrial homeostasis and cardiomyocyte survival. *J Cell Sci* 129: 3705–3720, 2016. doi:10.1242/jcs.192203.
69. **Naon D**, **Zaninello M**, **Giacomello M**, **Varanita T**, **Grespi F**, **Lakshminaranayan S**, **Serafini A**, **Semenzato M**, **Herkenne S**, **Hernandez-Alvarez MI**, **Zorzano A**, **De Stefani D**, **Dorn GW 2nd**, **Scorrano L.** Critical reappraisal confirms that Mitofusin 2 is an endoplasmic reticulum-mitochondria tether. *Proc Natl Acad Sci USA* 113: 11249–11254, 2016. doi:10.1073/pnas.1606786113.
70. **Filadi R**, **Greotti E**, **Turacchio G**, **Luini A**, **Pozzan T**, **Pizzo P.** Mitofusin 2 ablation increases endoplasmic reticulum-mitochondria coupling. *Proc Natl Acad Sci USA* 112: E2174–2181, 2015. doi:10.1073/pnas.1504880112.
71. **Cosson P**, **Marchetti A**, **Ravazzola M**, **Orci L.** Mitofusin-2 independent juxtaposition of endoplasmic reticulum and mitochondria: an ultrastructural study. *PLoS One* 7: e46293, 2012. doi:10.1371/journal.pone.0046293.
72. **Naon D**, **Zaninello M**, **Giacomello M**, **Varanita T**, **Grespi F**, **Lakshminaranayan S**, **Serafini A**, **Semenzato M**, **Herkenne S**, **Hernandez-Alvarez MI**, **Zorzano A**, **De Stefani D**, **Dorn GW 2nd**, **Scorrano L.** Reply to Filadi et al.: does mitofusin 2 tether or separate endoplasmic reticulum and mitochondria? *Proc Natl Acad Sci USA* 114: E2268–E2269, 2017. doi:10.1073/pnas.1618610114.
73. **Filadi R**, **Greotti E**, **Turacchio G**, **Luini A**, **Pozzan T**, **Pizzo P.** On the role of Mitofusin 2 in endoplasmic reticulum-mitochondria tethering. *Proc Natl Acad Sci USA* 114: E2266–E2267, 2017. doi:10.1073/pnas.1616040114.
74. **Chen Y**, **Csordas G**, **Jowdy C**, **Schneider TG**, **Csordas N**, **Wang W**, **Liu Y**, **Kohlhaas M**, **Meiser M**, **Bergem S**, **Nerbonne JM**, **Dorn GW 2nd**, **Maack C.** Mitofusin 2-containing mitochondrial-reticular microdomains direct rapid cardiomyocyte bioenergetic responses via interorganelle Ca^{2+} crosstalk. *Circ Res* 111: 863–875, 2012. doi:10.1161/CIRCRESAHA.112.266585.
75. **Casellas-Diaz S**, **Larramona-Arcas R**, **Rique-Pujol G**, **Tena-Morraja P**, **Muller-Sanchez C**, **Segarra-Mondejar M**, **Gavalda-Navarro A**, **Villarroya F**, **Reina M**, **Martinez-Estrada OM**, **Soriano FX.** Mfn2 localization in the ER is necessary for its bioenergetic function and neuritic development. *EMBO Rep* 22: e51954, 2021. doi:10.15252/embr.202051954.
76. **Zhang H**, **Bryson VG**, **Wang C**, **Li T**, **Kerr JP**, **Wilson R**, **Muoio DM**, **Bloch RJ**, **Ward C**, **Rosenberg PB.** Desmin interacts with STIM1 and coordinates Ca2+ signaling in skeletal muscle. *JCI Insight* 6: e143472, 2021. doi:10.1172/jci.insight.143472.
77. **Dayal AA**, **Medvedeva NV**, **Nekrasova TM**, **Duhalin SD**, **Surin AK**, **Minin AA.** Desmin interacts directly with mitochondria. *Int J Mol Sci* 21: 8122, 2020. doi:10.3390/ijms21218122.
78. **Nishizawa M**, **Izawa I**, **Inoko A**, **Hayashi Y**, **Nagata K**, **Yokoyama T**, **Usukura J**, **Inagaki M.** Identification of trichoplein, a novel keratin filament-binding protein. *J Cell Sci* 118: 1081–1090, 2005. doi:10.1242/jcs.01667.
79. **Anesti V**, **Scorrano L.** The relationship between mitochondrial shape and function and the cytoskeleton. *Biochim Biophys Acta* 1757: 692–699, 2006. doi:10.1016/j.bbabio.2006.04.013.
80. **Rezniczek GA**, **Abrahamsberg C**, **Fuchs P**, **Spazierer D**, **Wiche G.** Plectin 5'-transcript diversity: short alternative sequences determine stability of gene products, initiation of translation and subcellular localization of isoforms. *Hum Mol Genet* 12: 3181–3194, 2003. doi:10.1093/hmg/ddg345.
81. **Konieczny P**, **Fuchs P**, **Reipert S**, **Kunz WS**, **Zeold A**, **Fischer I**, **Paulin D**, **Schroder R**, **Wiche G.** Myofiber integrity depends on desmin network targeting to Z-disks and costameres via distinct plectin isoforms. *J Cell Biol* 181: 667–681, 2008. doi:10.1083/jcb.200711058.
82. **Winter L**, **Abrahamsberg C**, **Wiche G.** Plectin isoform 1b mediates mitochondrion-intermediate filament network linkage and controls organelle shape. *J Cell Biol* 181: 903–911, 2008. doi:10.1083/jcb.200710151.
83. **Baek A**, **Son S**, **Baek YM**, **Kim DE.** KRT8 (keratin 8) attenuates necrotic cell death by facilitating mitochondrial fission-mediated mitophagy through interaction with PLEC (plectin). *Autophagy* 17: 3939–3956, 2021. doi:10.1080/15548627.2021.1897962.
84. **Roediger WE.** The colonic epithelium in ulcerative colitis: an energy-deficiency disease? *Lancet* 2: 712–715, 1980. doi:10.1016/s0140-6736(80)91934-0.

85. **Rath E**, **Haller D.** Intestinal epithelial cell metabolism at the interface of microbial dysbiosis and tissue injury. *Mucosal Immunol* 15: 595–604, 2022. doi:10.1038/s41385-022-00514-x.
86. **Haberman Y**, **Karns R**, **Dexheimer PJ**, **Schirmer M**, **Somekh J**, **Jurickova I**, **et al.** Ulcerative colitis mucosal transcriptomes reveal mitochondriopathy and personalized mechanisms underlying disease severity and treatment response. *Nat Commun* 10: 38, 2019. doi:10.1038/s41467-018-07841-3.
87. **Sifroni KG**, **Damiani CR**, **Stoffel C**, **Cardoso MR**, **Ferreira GK**, **Jeremias IC**, **Rezin GT**, **Scaini G**, **Schuck PF**, **Dal-Pizzol F**, **Streck EL.** Mitochondrial respiratory chain in the colonic mucosal of patients with ulcerative colitis. *Mol Cell Biochem* 342: 111–115, 2010. doi:10.1007/s11010-010-0474-x.
88. **Khaloian S**, **Rath E**, **Hammoudi N**, **Gleisinger E**, **Blutke A**, **Giesbertz P**, **Berger E**, **Metwaly A**, **Waldschmitt N**, **Allez M**, **Haller D.** Mitochondrial impairment drives intestinal stem cell transition into dysfunctional Paneth cells predicting Crohn's disease recurrence. *Gut* 69: 1939–1951, 2020. doi:10.1136/gutjnl-2019-319514.
89. **Mottawea W**, **Chiang CK**, **Muhlbauer M**, **Starr AE**, **Butcher J**, **Abujamel T**, **Deeke SA**, **Brandel A**, **Zhou H**, **Shokralla S**, **Hajibabaei M**, **Singleton R**, **Benchimol EI**, **Jobin C**, **Mack DR**, **Figeys D**, **Stintzi A.** Altered intestinal microbiota-host mitochondria crosstalk in new onset Crohn's disease. *Nat Commun* 7: 13419, 2016. doi:10.1038/ncomms13419.
90. **De Preter V**, **Arijs I**, **Windey K**, **Vanhove W**, **Vermeire S**, **Schuit F**, **Rutgeerts P**, **Verbeke K.** Impaired butyrate oxidation in ulcerative colitis is due to decreased butyrate uptake and a defect in the oxidation pathway. *Inflamm Bowel Dis* 18: 1127–1136, 2012. doi:10.1002/ibd.21894.